

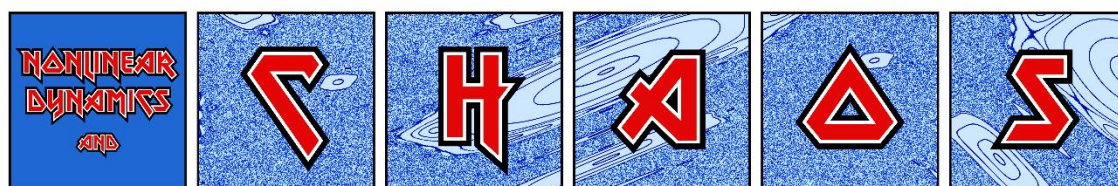
# Numerical methods of chaos detection

**Haris Skokos**

**Nonlinear Dynamics and Chaos (NDC) group**  
**Department of Mathematics and Applied Mathematics**  
**University of Cape Town**  
**Cape Town, South Africa**

**E-mail: [haris.skokos@uct.ac.za](mailto:haris.skokos@uct.ac.za) – [haris.skokos@gmail.com](mailto:haris.skokos@gmail.com)**  
**URL: [http://math\\_research.uct.ac.za/~hskokos/](http://math_research.uct.ac.za/~hskokos/)**

**Mathematics Seminar, Khalifa University**  
**4 June 2025, Abu Dhabi, United Arab Emirates**



# Outline

- **Dynamical Systems**
  - ✓ **Hamiltonian models – Variational equations**
  - ✓ **Symplectic maps – Tangent map**
- **Brief presentation of chaos detection methods**
- **Chaos Indicators**
  - ✓ **Lyapunov exponents**
  - ✓ **Smaller ALignment Index – SALI**
    - **Definition**
    - **Behavior for chaotic and regular motion**
    - **Applications**
  - ✓ **Generalized ALignment Index – GALI**
    - **Definition - Relation to SALI**
    - **Behavior for chaotic and regular motion**
    - **Application to time-dependent and dissipative models**
- **Chaos diagnostics based on Lagrangian descriptors (LDs)**
- **Summary**

# Autonomous Hamiltonian systems

Consider an **N degree of freedom** autonomous Hamiltonian system having a Hamiltonian function of the form:

$$H(\overbrace{q_1, q_2, \dots, q_N}^{\text{positions}}, \overbrace{p_1, p_2, \dots, p_N}^{\text{momenta}})$$

The time evolution of an orbit (trajectory) with initial condition

$$P(0) = (q_1(0), q_2(0), \dots, q_N(0), p_1(0), p_2(0), \dots, p_N(0))$$

is governed by the **Hamilton's equations of motion**

$$\frac{dp_i}{dt} = -\frac{\partial H}{\partial q_i}, \quad \frac{dq_i}{dt} = \frac{\partial H}{\partial p_i}$$

# Variational Equations

We use the notation  $\mathbf{x} = (q_1, q_2, \dots, q_N, p_1, p_2, \dots, p_N)^T$ . The **deviation vector** from a given orbit is denoted by

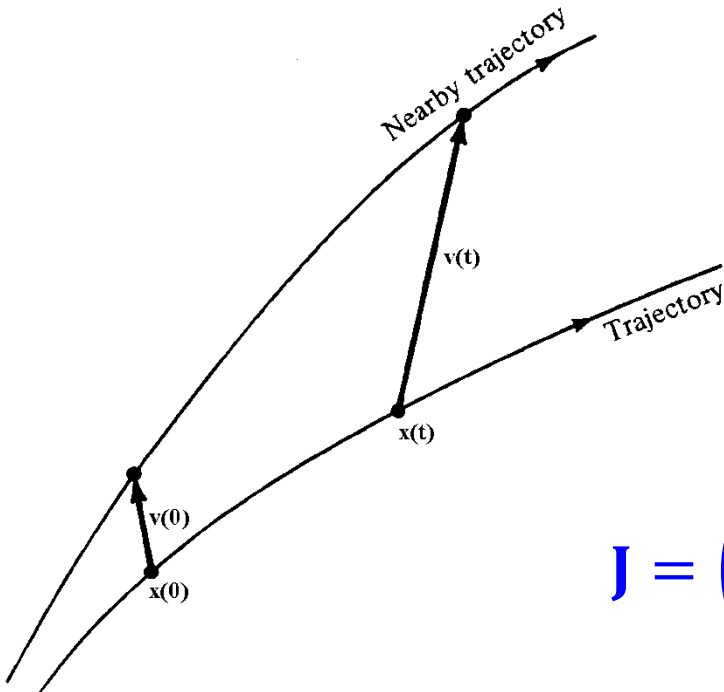
$$\mathbf{v} = (\delta x_1, \delta x_2, \dots, \delta x_n)^T, \text{ with } n=2N$$

The time evolution of  $\mathbf{v}$  is given by the so-called **variational equations**:

$$\frac{d\mathbf{v}}{dt} = -\mathbf{J} \cdot \mathbf{P} \cdot \mathbf{v}$$

where

$$\mathbf{J} = \begin{pmatrix} \mathbf{0}_N & -\mathbf{I}_N \\ \mathbf{I}_N & \mathbf{0}_N \end{pmatrix}, \mathbf{P}_{ij} = \frac{\partial^2 H}{\partial x_i \partial x_j} \quad i, j = 1, 2, \dots, n$$





# Symplectic Maps

Consider an **2N-dimensional symplectic map T**. In this case we have **discrete time**.

The evolution of an **orbit** with initial condition

$$P(0)=(x_1(0), x_2(0), \dots, x_{2N}(0))$$

is governed by the **equations of map T**

$$P(i+1)=T P(i) \text{ , } i=0,1,2,\dots$$

The evolution of an initial **deviation vector**

$$v(0) = (\delta x_1(0), \delta x_2(0), \dots, \delta x_{2N}(0))$$

is given by the corresponding **tangent map**

$$v(i+1) = \left. \frac{\partial T}{\partial P} \right|_i \cdot v(i) \text{ , } i = 0, 1, 2, \dots$$

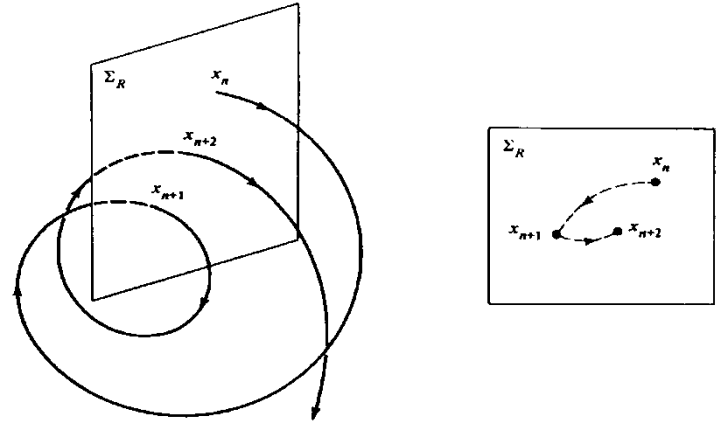
# Chaos detection techniques

- **Based on the visualization of orbits**
  - ✓ **Poincaré Surface of Section (PSS)**
  - ✓ **the color and rotation (CR) method**
  - ✓ **the 3D phase space slices (3PSS) technique**

# Poincaré Surface of Section (PSS)

We can constrain the study of an  $N+1$  degree of freedom Hamiltonian system to a **2N-dimensional subspace of the general phase space**.

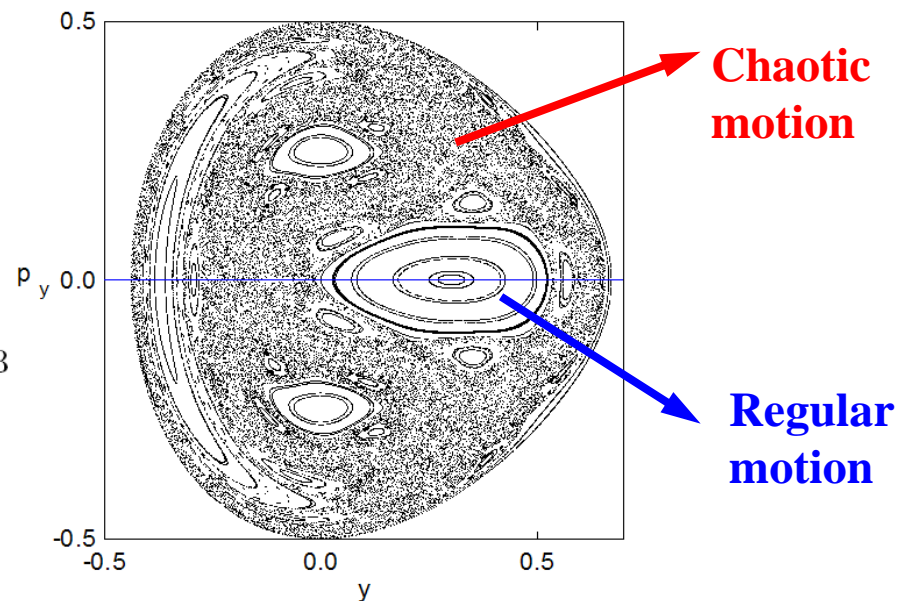
In this sense an  $N+1$  degree of freedom Hamiltonian system corresponds to a **2N-dimensional symplectic map**.



Lieberman & Lichtenberg, 1992, *Regular and Chaotic Dynamics*, Springer.

**The 2D Hénon-Heiles system:**

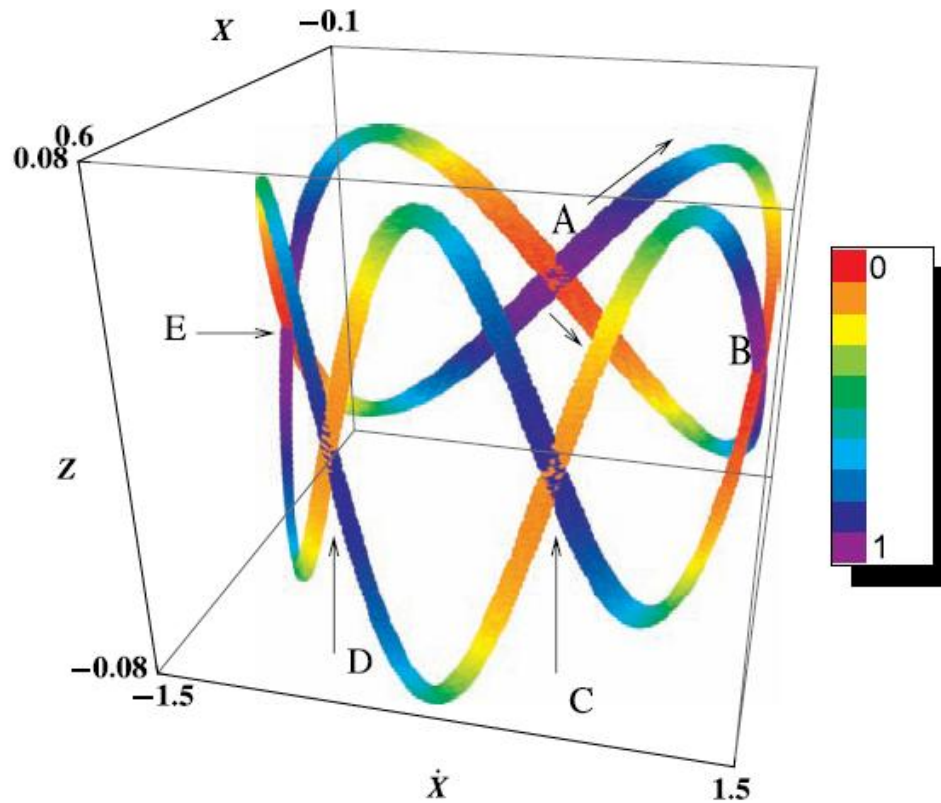
$$H_2 = \frac{1}{2}(p_x^2 + p_y^2) + \frac{1}{2}(x^2 + y^2) + x^2y - \frac{1}{3}y^3$$



# The color and rotation (CR) method

For 3 degree of freedom Hamiltonian systems and 4 dimensional symplectic maps:

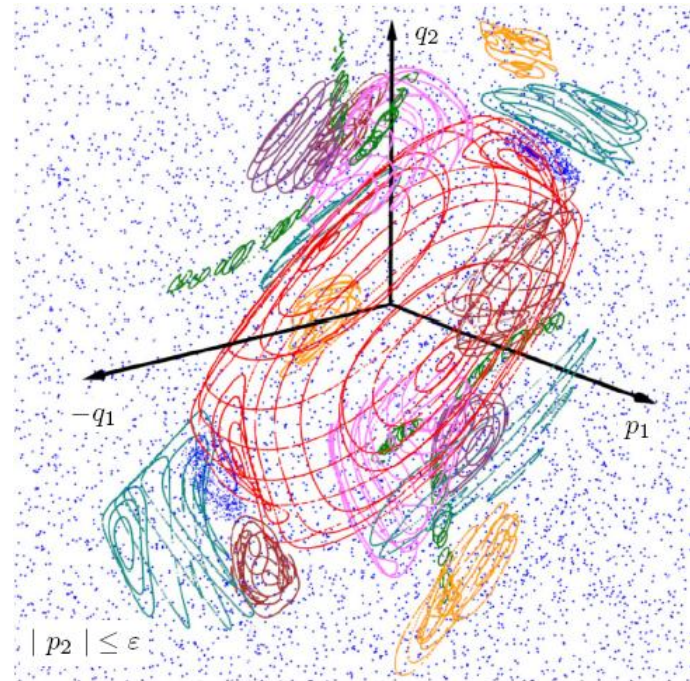
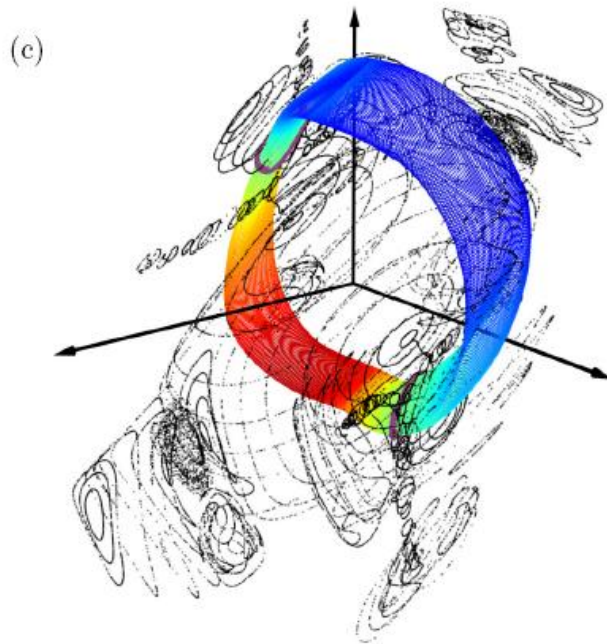
**We consider the 3D projection of the PSS and use color to indicate the 4<sup>th</sup> dimension.**



# The 3D phase space slices (3PSS) technique

For 3 degree of freedom Hamiltonian systems and 4 dimensional symplectic maps:

**We consider thin 3D phase space slices of the 4D phase space (e.g.  $|p_2| \leq \varepsilon$ ) and present intersections of orbits with these slices.**



# Chaos detection techniques

- **Based on the visualization of orbits**
  - ✓ Poincaré Surface of Section (PSS)
  - ✓ the color and rotation (CR) method
  - ✓ the 3D phase space slices (3PSS) technique
- **Based on the numerical analysis of orbits**
  - ✓ Frequency Map Analysis
  - ✓ 0-1 test

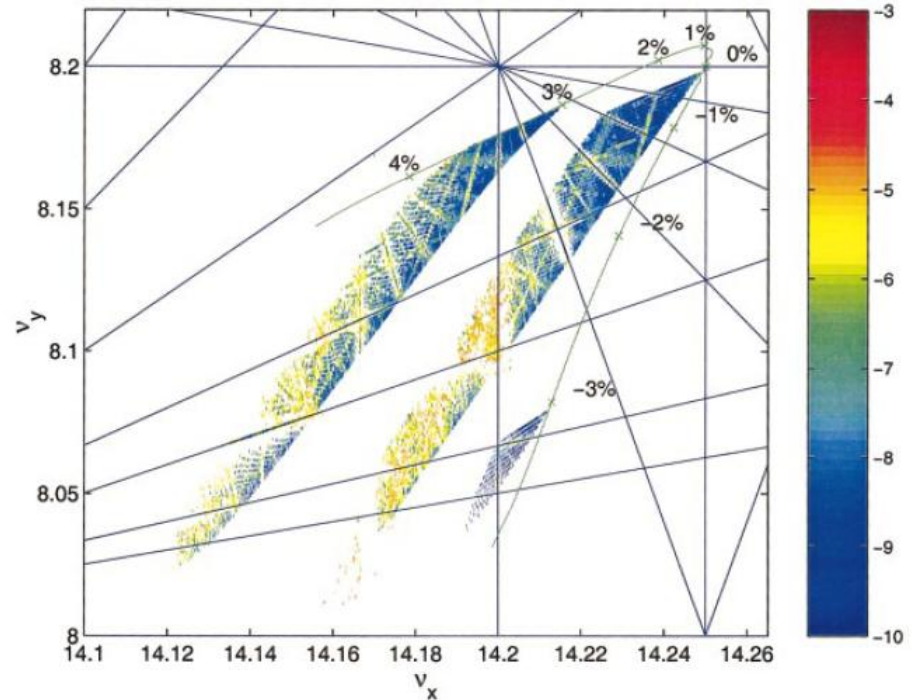
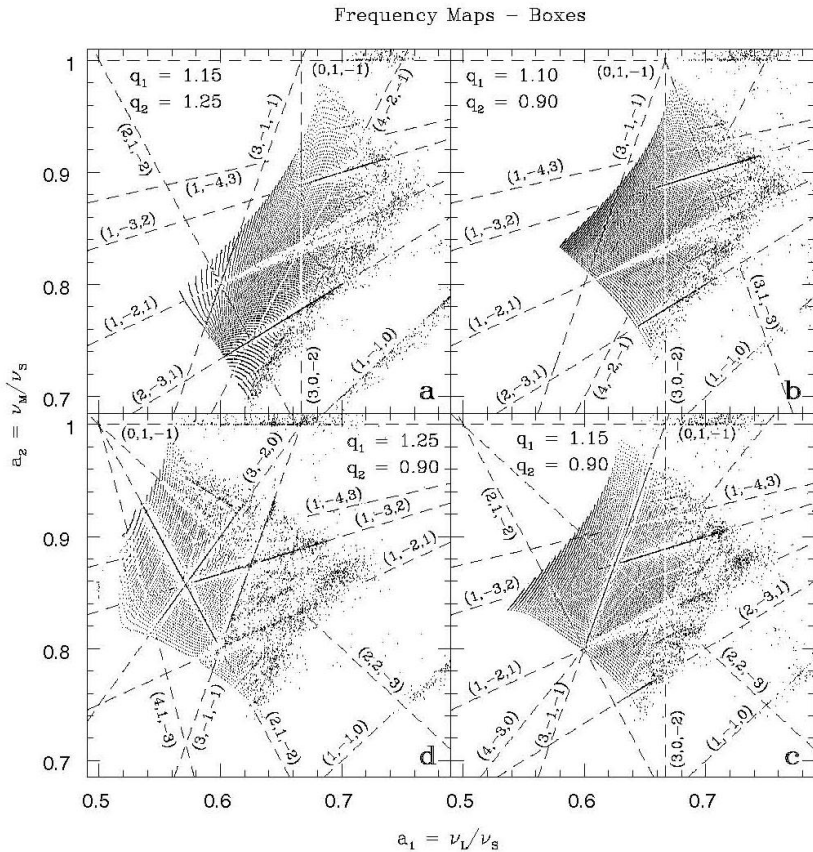


# Frequency Map Analysis

Create **Frequency Maps** by computing the fundamental frequencies of orbits.

## Regular motion: The computed frequencies do not vary in time

## Chaotic motion: The computed frequencies vary in time



Steier et al., Phys. Rev. E (2002)

**Papaphilippou & Laskar, Astron. Astrophys. (1998)**

# Chaos detection techniques

- **Based on the visualization of orbits**
  - ✓ **Poincaré Surface of Section (PSS)**
  - ✓ **the color and rotation (CR) method**
  - ✓ **the 3D phase space slices (3PSS) technique**
- **Based on the numerical analysis of orbits**
  - ✓ **Frequency Map Analysis**
  - ✓ **0-1 test**
- **Chaos indicators based on the evolution of deviation vectors from a given orbit**
  - ✓ **Maximum Lyapunov Exponent (MLE)**
  - ✓ **Fast Lyapunov Indicator (FLI) and Orthogonal Fast Lyapunov Indicators (OFLI and OFLI2)**
  - ✓ **Mean Exponential Growth Factor of Nearby Orbits (MEGNO)**
  - ✓ **Relative Lyapunov Indicator (RLI)**
  - ✓ **Smaller ALignment Index – SALI**
  - ✓ **Generalized ALignment Index – GALI**



# Maximum Lyapunov Exponent (MLE)

Chaos: sensitive dependence on initial conditions.

Roughly speaking, the MLE of a given orbit characterizes the **mean exponential rate of divergence** of trajectories surrounding it.

Consider an orbit in the  $2N$ -dimensional phase space with **initial condition  $\mathbf{x}(0)$**  and **an initial deviation vector (small perturbation) from it  $\mathbf{v}(0)$** .

Then the mean exponential rate of divergence is:

$$\text{MLE} = \lambda_1 = \lim_{t \rightarrow \infty} \Lambda(t) = \lim_{t \rightarrow \infty} \frac{1}{t} \ln \frac{\|\mathbf{v}(t)\|}{\|\mathbf{v}(0)\|}$$

$\lambda_1 = 0 \rightarrow$  Regular motion ( $\Lambda \propto t^{-1}$ )

$\lambda_1 > 0 \rightarrow$  Chaotic motion

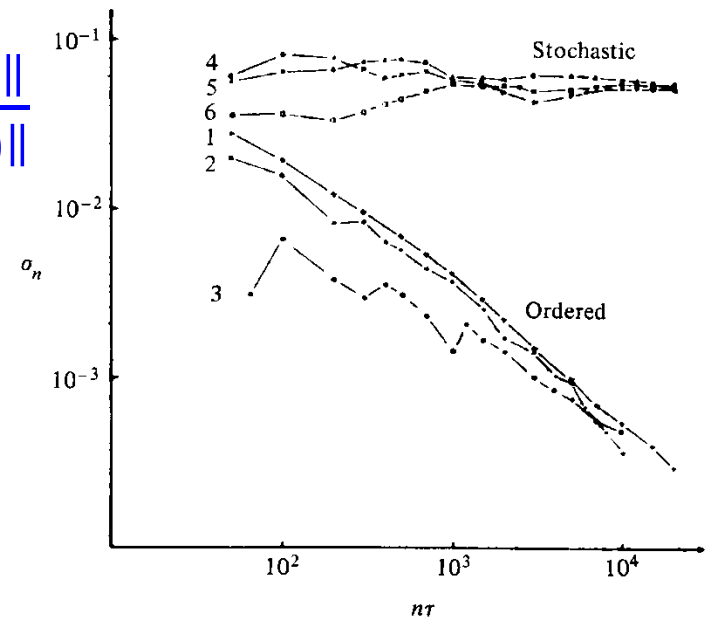


Figure 5.7. Behavior of  $\sigma_n$  at the intermediate energy  $E = 0.125$  for initial points taken in the ordered (curves 1–3) or stochastic (curves 4–6) regions (after Benettin *et al.*, 1976).

**The  
Smaller ALignment Index  
(SALI)  
method**

# Definition of the SALI

We follow the evolution in time of two different initial deviation vectors ( $\mathbf{v}_1(0)$ ,  $\mathbf{v}_2(0)$ ), and define SALI [S., J. Phys. A (2001) – S. & Manos, Lect. Notes Phys. (2016)] as:

$$\text{SALI}(\mathbf{t}) = \min\{\|\hat{\mathbf{v}}_1(\mathbf{t}) + \hat{\mathbf{v}}_2(\mathbf{t})\|, \|\hat{\mathbf{v}}_1(\mathbf{t}) - \hat{\mathbf{v}}_2(\mathbf{t})\|\}$$

where

$$\hat{\mathbf{v}}_1(\mathbf{t}) = \frac{\mathbf{v}_1(\mathbf{t})}{\|\mathbf{v}_1(\mathbf{t})\|}$$

When the two vectors become collinear

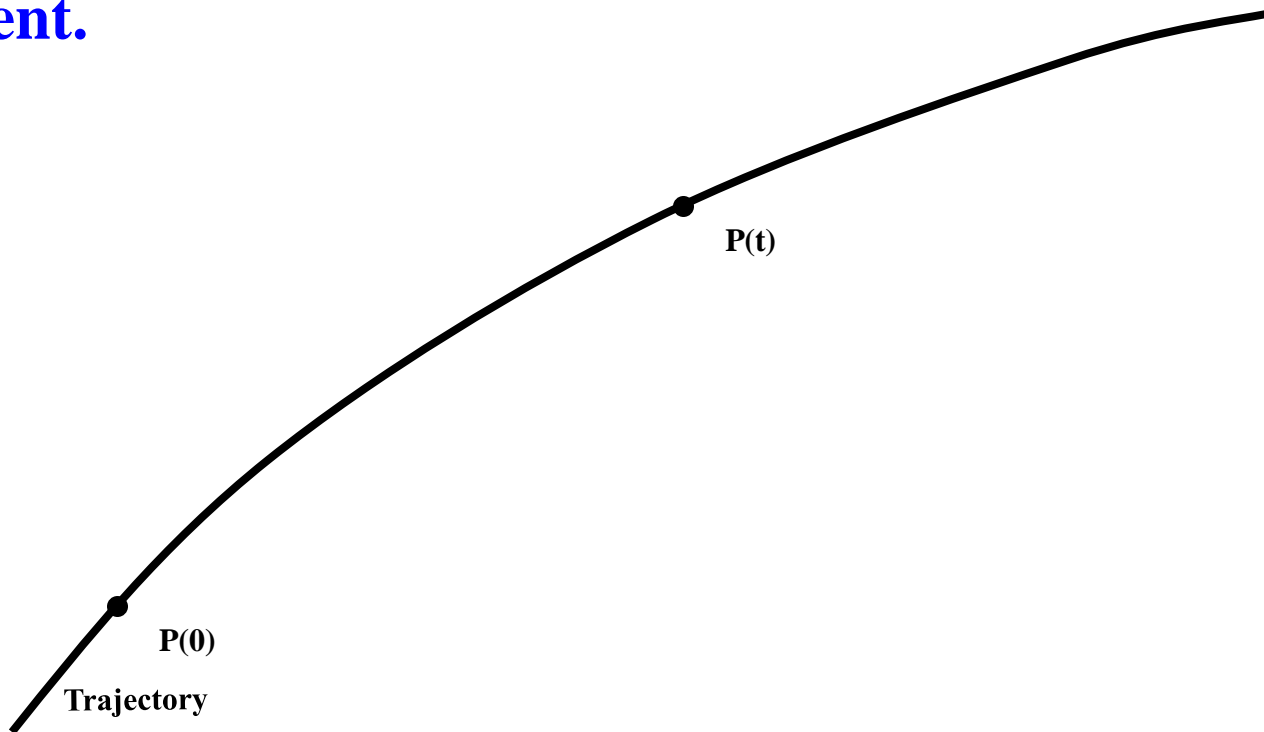
$$\text{SALI}(\mathbf{t}) \rightarrow 0$$

# Behavior of SALI for **chaotic motion**

For chaotic orbits the two initially different deviation vectors tend to coincide with the direction defined by the maximum Lyapunov exponent.

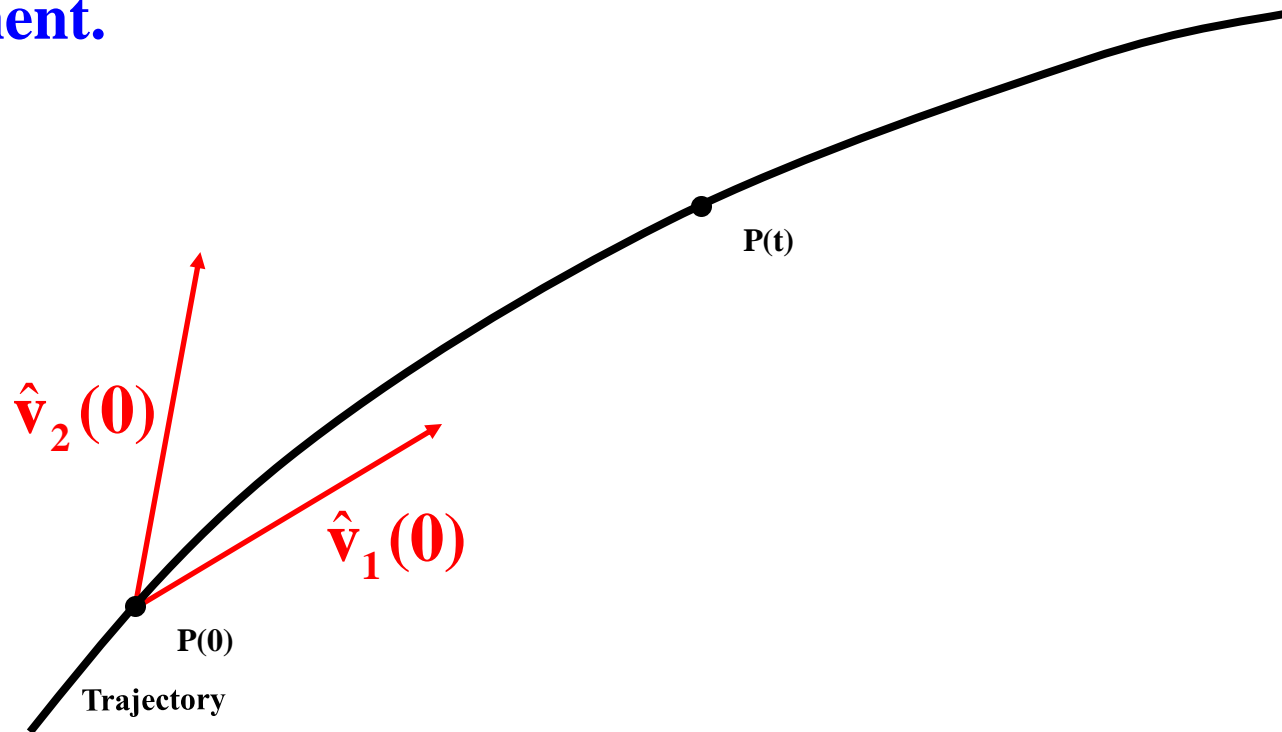
# Behavior of SALI for **chaotic motion**

For chaotic orbits the two initially different deviation vectors tend to coincide with the direction defined by the maximum Lyapunov exponent.



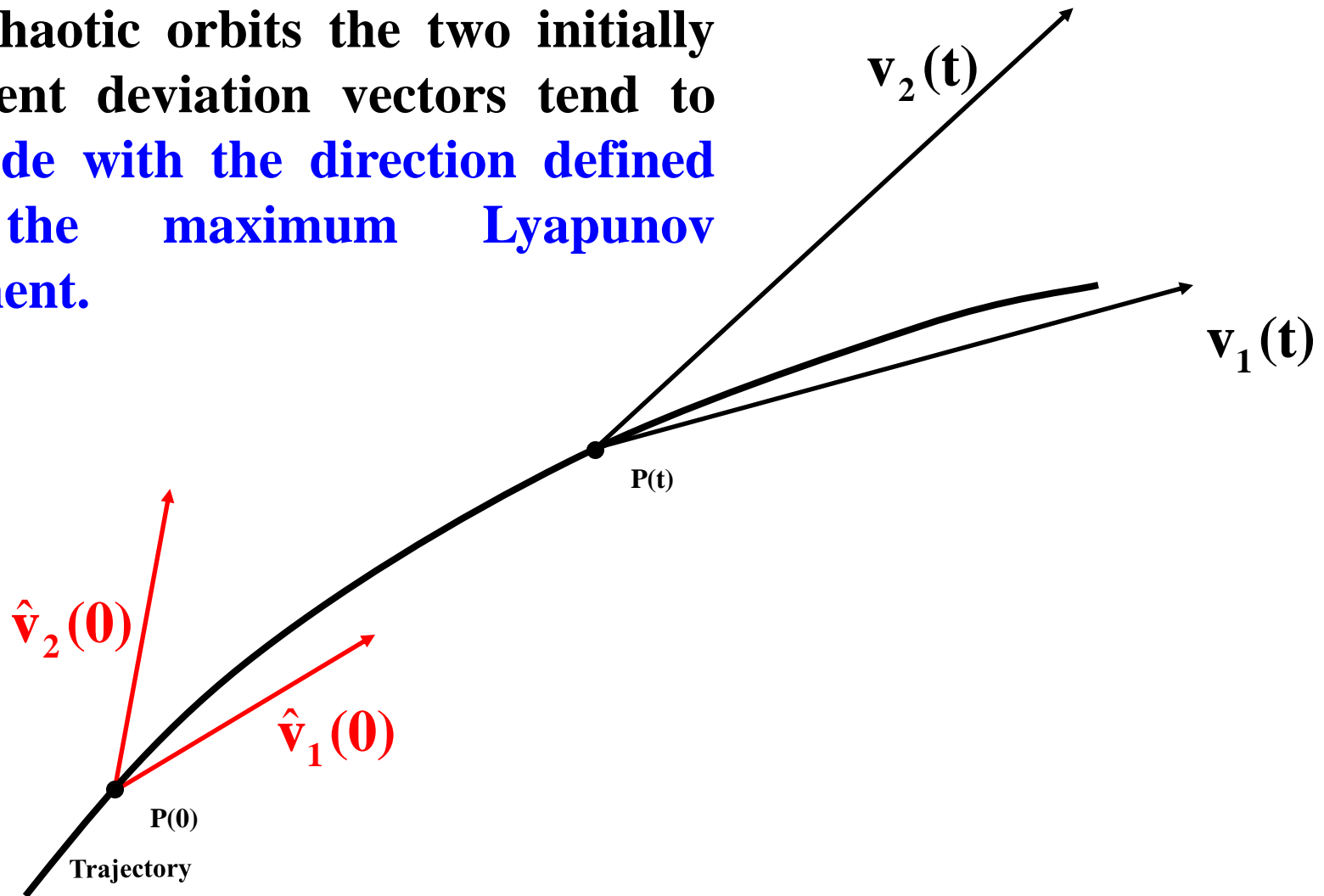
# Behavior of SALI for **chaotic motion**

For chaotic orbits the two initially different deviation vectors tend to coincide with the direction defined by the maximum Lyapunov exponent.



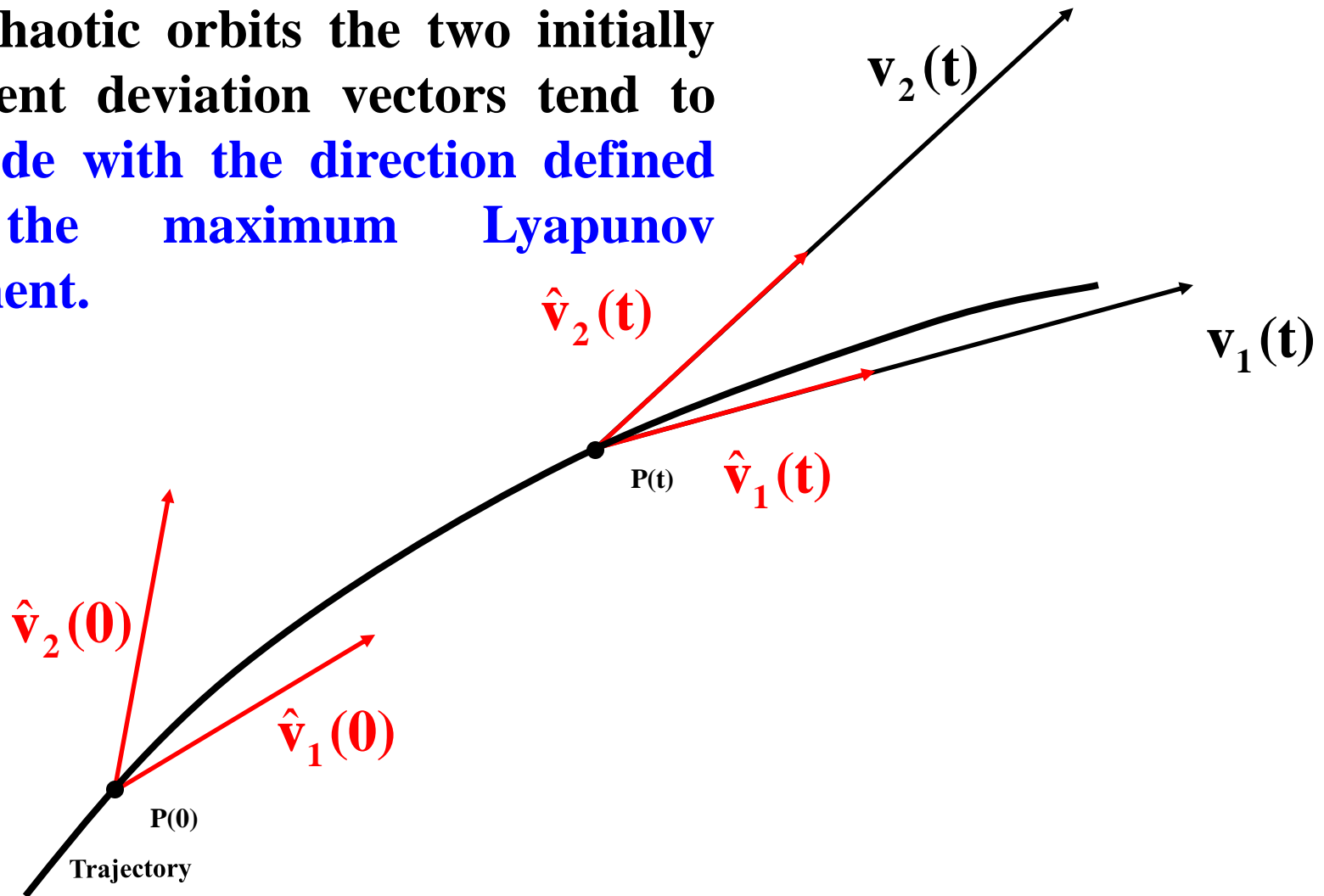
# Behavior of SALI for **chaotic motion**

For chaotic orbits the two initially different deviation vectors tend to coincide with the direction defined by the maximum Lyapunov exponent.



# Behavior of SALI for **chaotic motion**

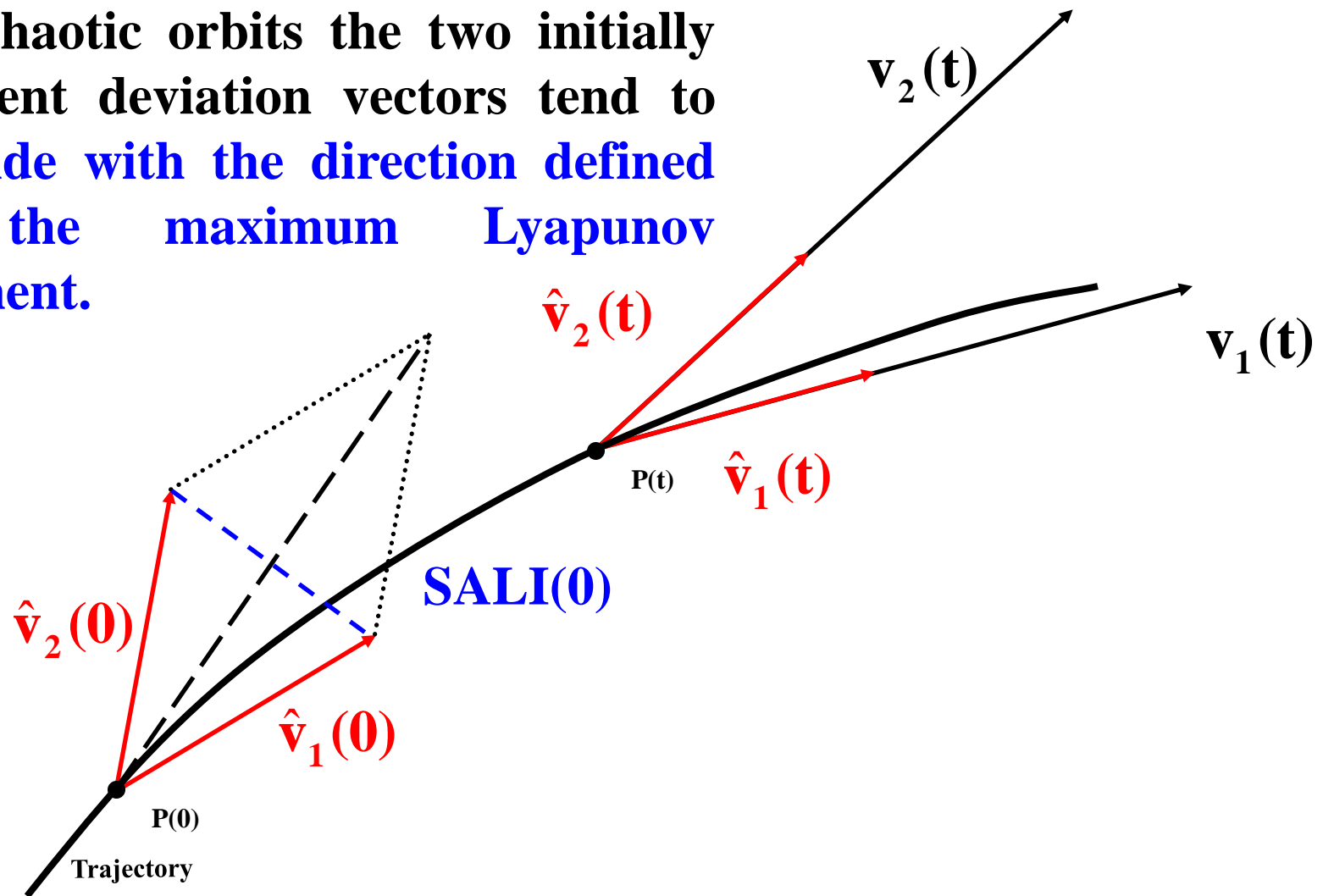
For chaotic orbits the two initially different deviation vectors tend to coincide with the direction defined by the maximum Lyapunov exponent.





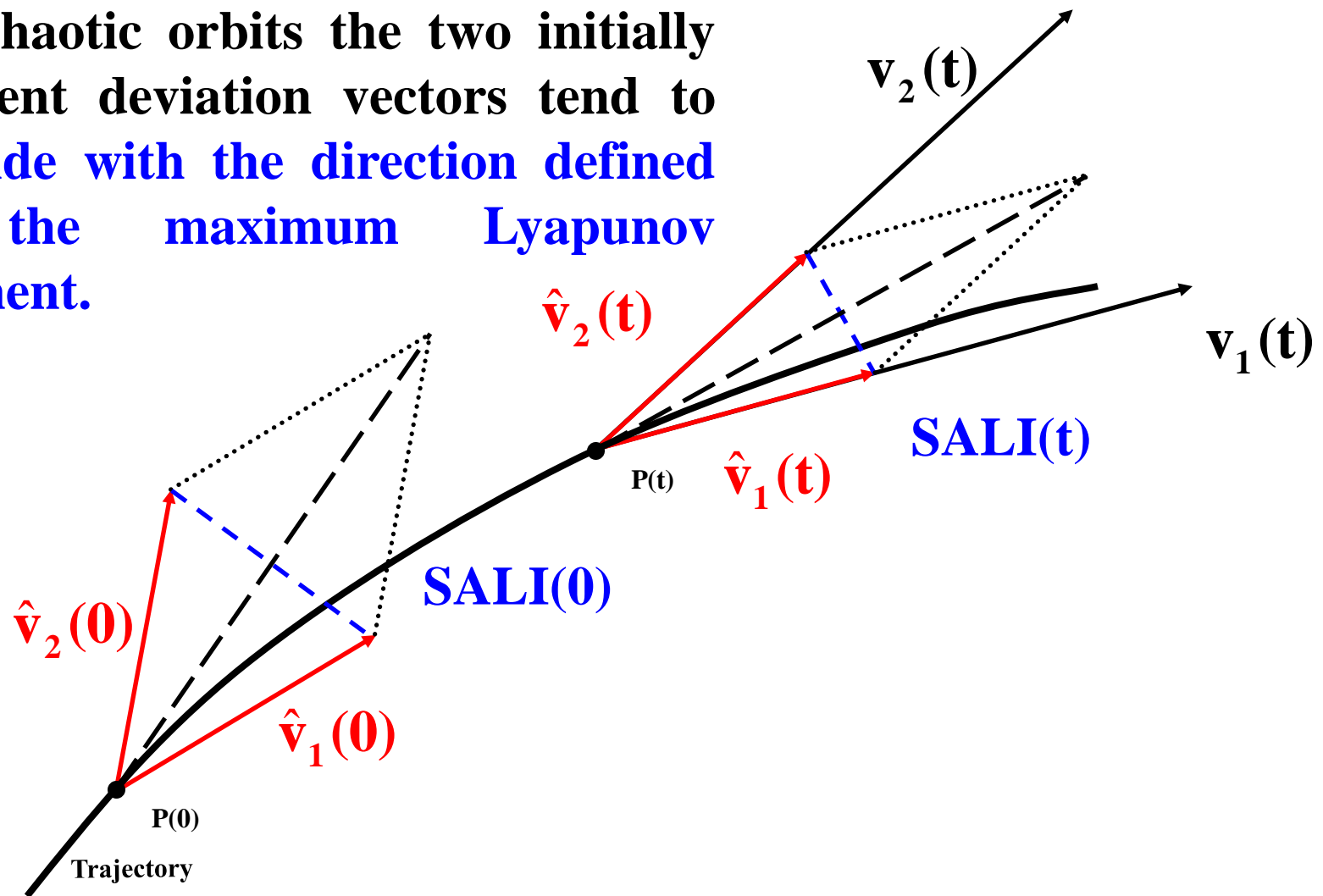
# Behavior of SALI for **chaotic motion**

For chaotic orbits the two initially different deviation vectors tend to coincide with the direction defined by the maximum Lyapunov exponent.



# Behavior of SALI for **chaotic motion**

For chaotic orbits the two initially different deviation vectors tend to coincide with the direction defined by the maximum Lyapunov exponent.

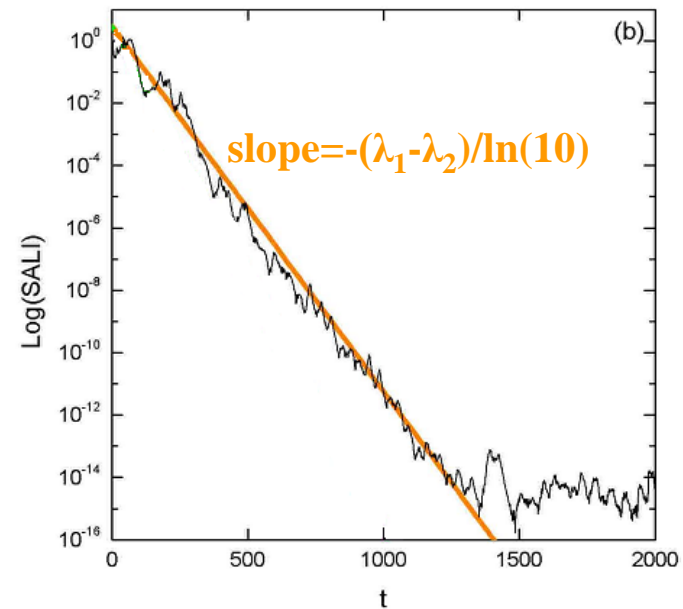
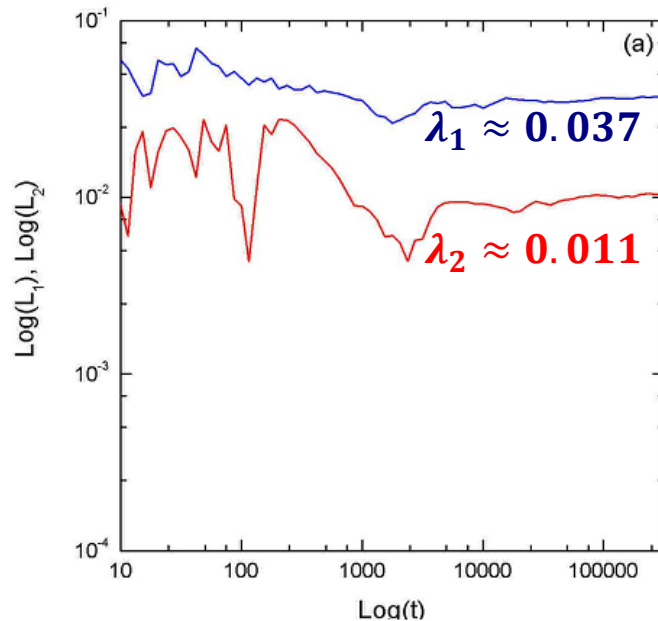


# Behavior of the SALI for **chaotic motion**

We test the validity of the approximation  $\text{SALI} \propto e^{-(\lambda_1 - \lambda_2)t}$  [S. et al., J. Phys. A (2004)] for a chaotic orbit of the 3D Hamiltonian

$$H = \sum_{i=1}^3 \frac{\omega_i}{2} (q_i^2 + p_i^2) + q_1^2 q_2 + q_1^2 q_3$$

with  $\omega_1=1$ ,  $\omega_2=1.4142$ ,  $\omega_3=1.7321$ ,  $H=0.09$

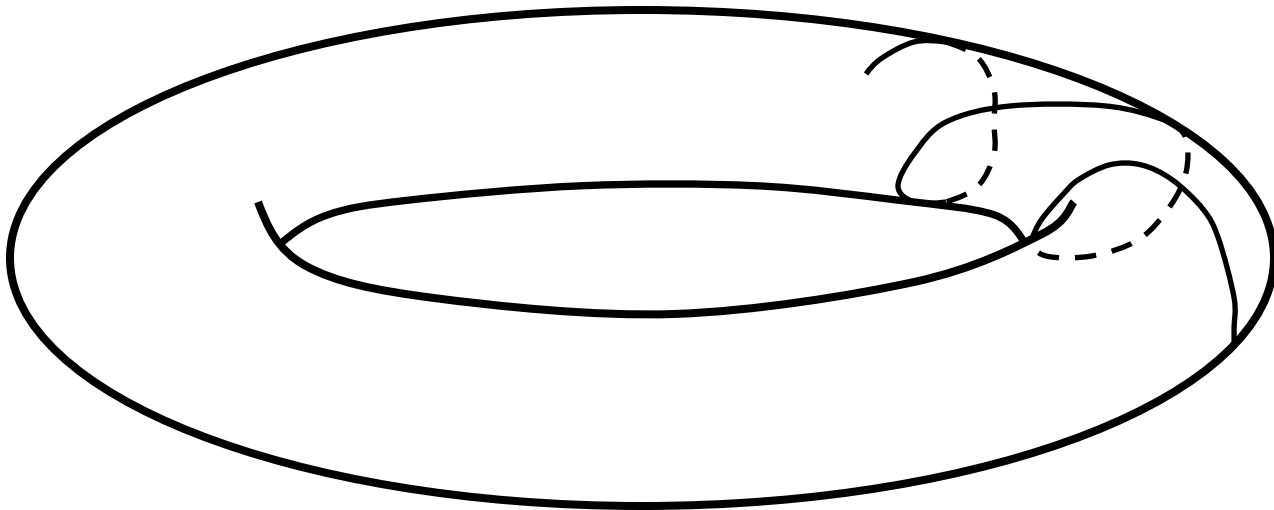


# Behavior of SALI for **regular motion**

Regular motion occurs on a torus and two different initial deviation vectors **become tangent to the torus, generally having different directions.**

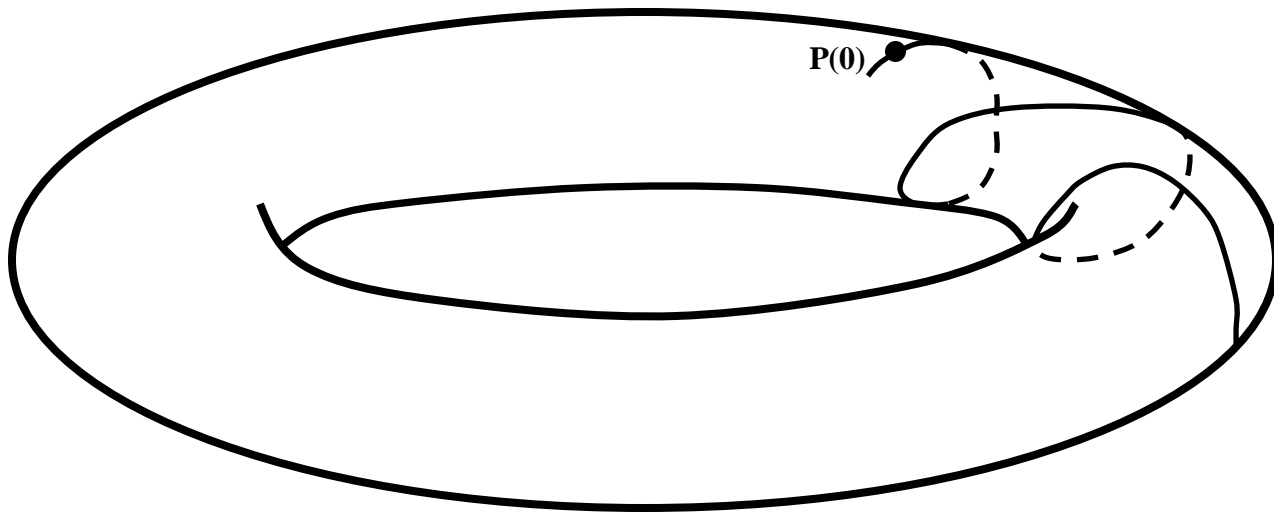
# Behavior of SALI for **regular motion**

Regular motion occurs on a torus and two different initial deviation vectors **become tangent to the torus, generally having different directions.**



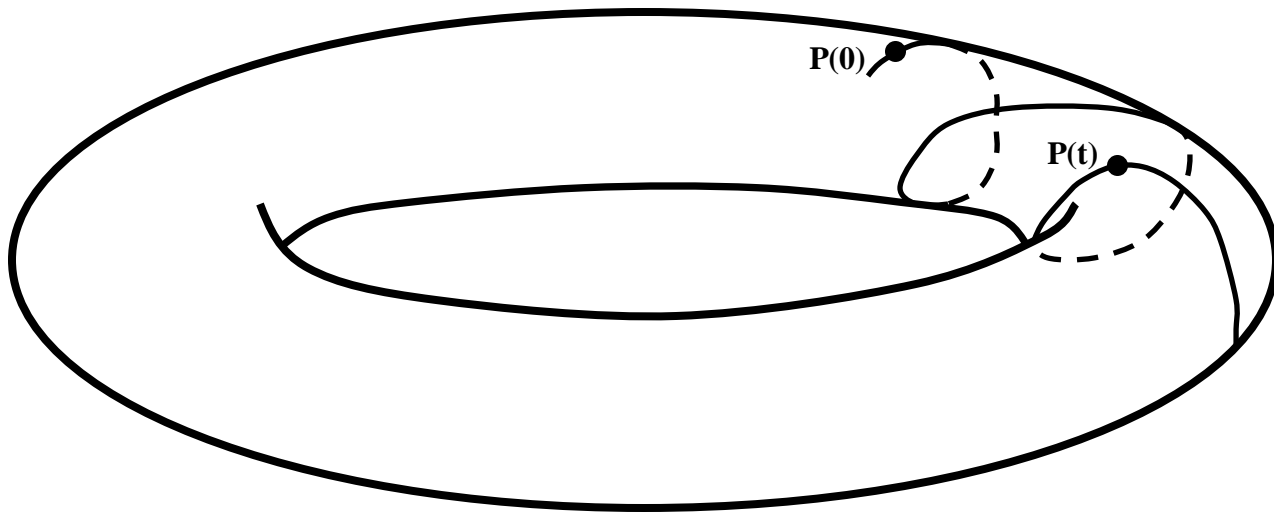
# Behavior of SALI for **regular motion**

Regular motion occurs on a torus and two different initial deviation vectors **become tangent to the torus, generally having different directions.**



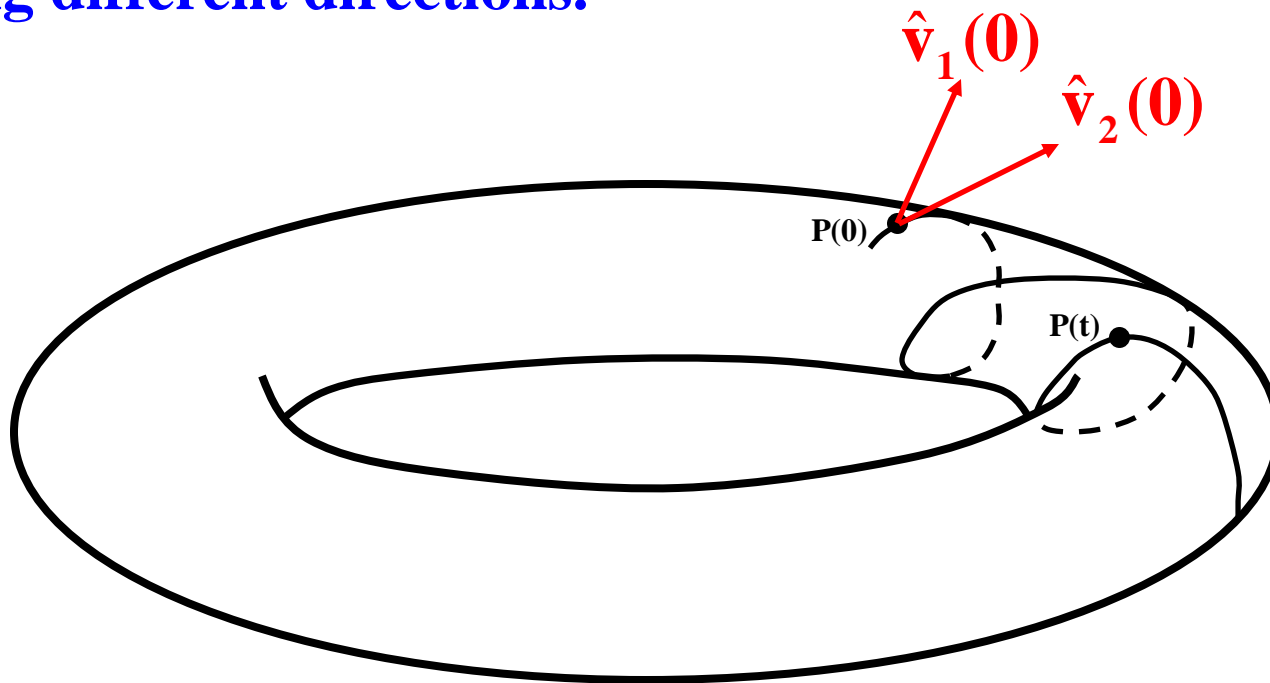
# Behavior of SALI for **regular motion**

Regular motion occurs on a torus and two different initial deviation vectors **become tangent to the torus, generally having different directions.**



# Behavior of SALI for **regular motion**

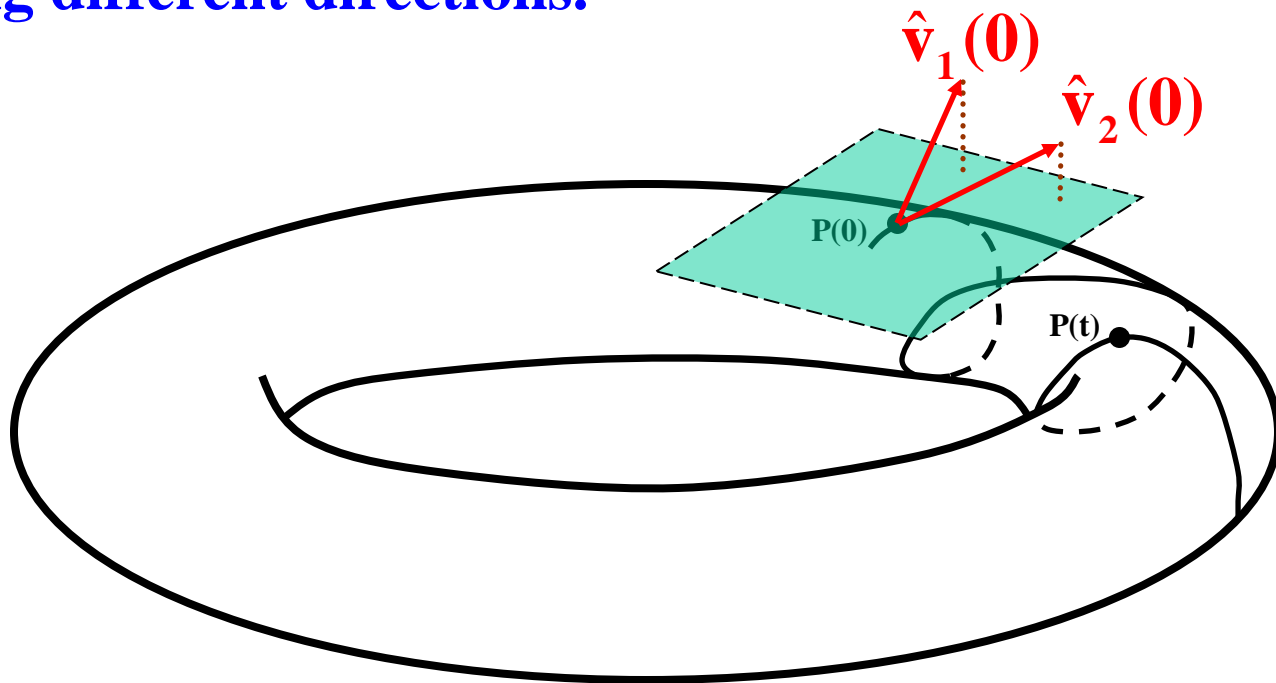
Regular motion occurs on a torus and two different initial deviation vectors **become tangent to the torus, generally having different directions.**





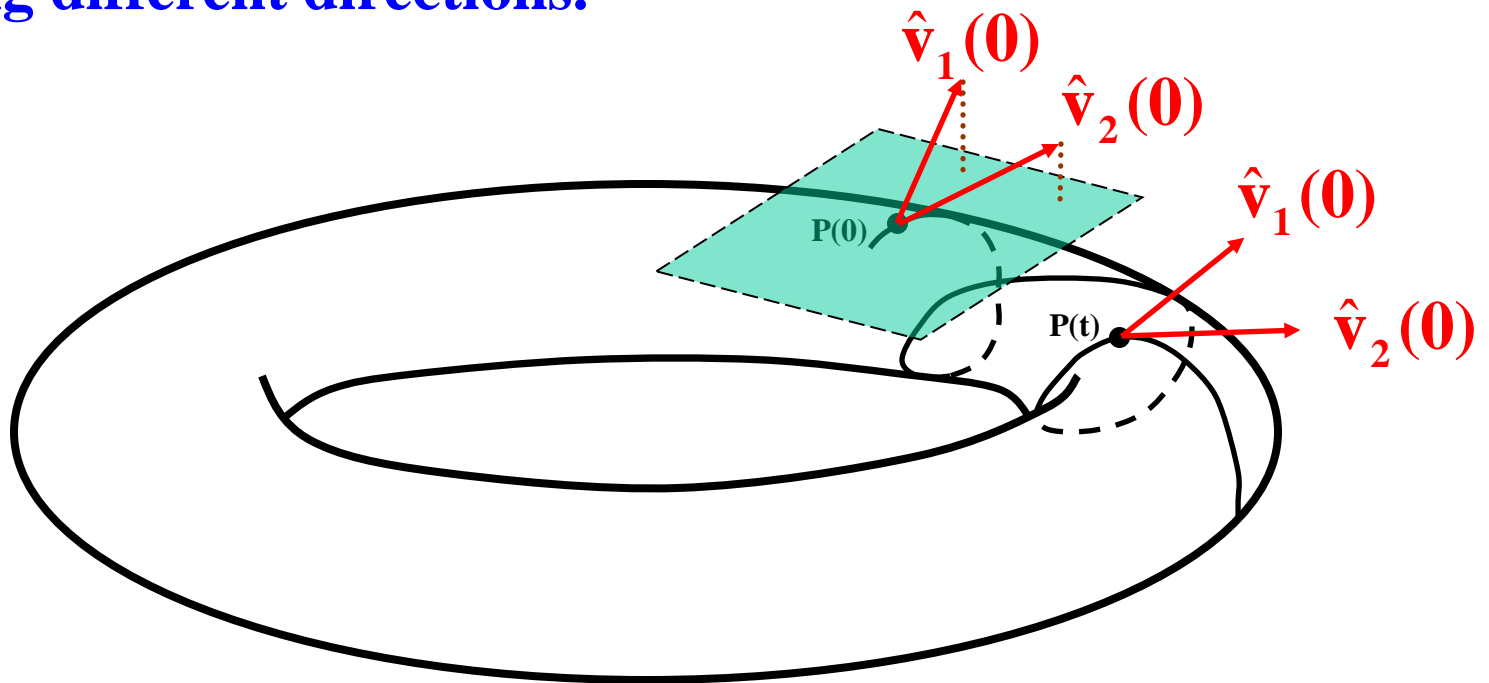
# Behavior of SALI for **regular motion**

Regular motion occurs on a torus and two different initial deviation vectors **become tangent to the torus**, generally **having different directions**.



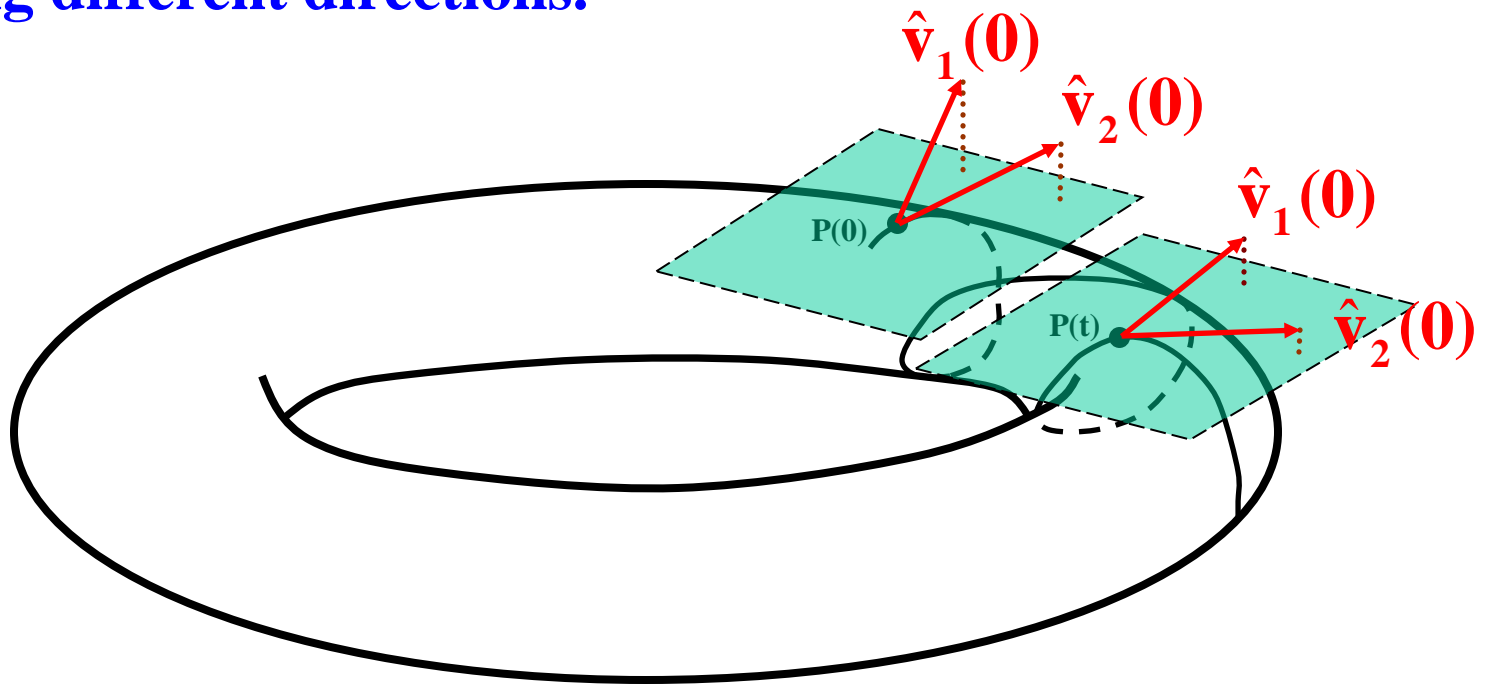
# Behavior of SALI for **regular motion**

Regular motion occurs on a torus and two different initial deviation vectors **become tangent to the torus, generally having different directions.**



# Behavior of SALI for **regular motion**

Regular motion occurs on a torus and two different initial deviation vectors **become tangent to the torus, generally having different directions.**



# SALI – Hénon-Heiles system

As an example, we consider the 2D Hénon-Heiles system:

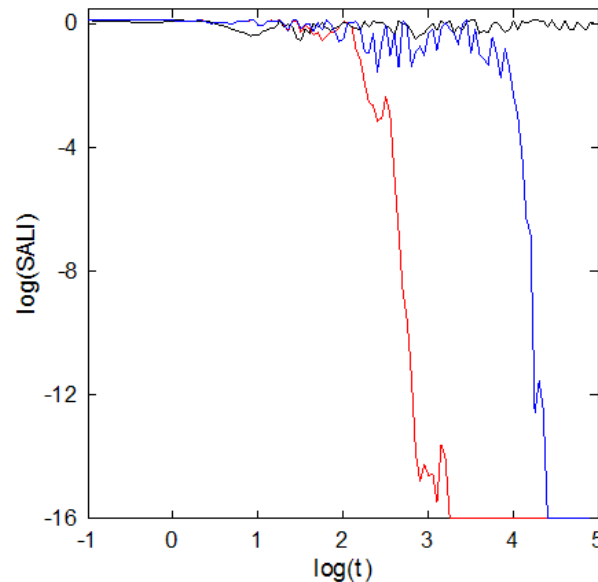
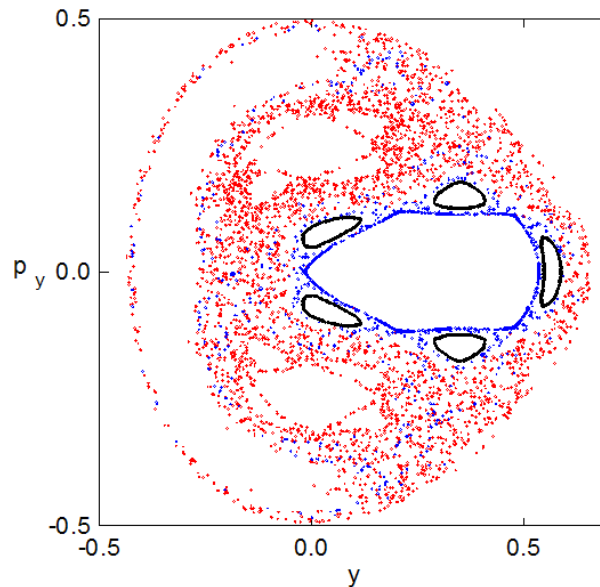
$$H = \frac{1}{2}(p_x^2 + p_y^2) + \frac{1}{2}(x^2 + y^2) + x^2y - \frac{1}{3}y^3$$

For  $E=1/8$  we consider the orbits with initial conditions:

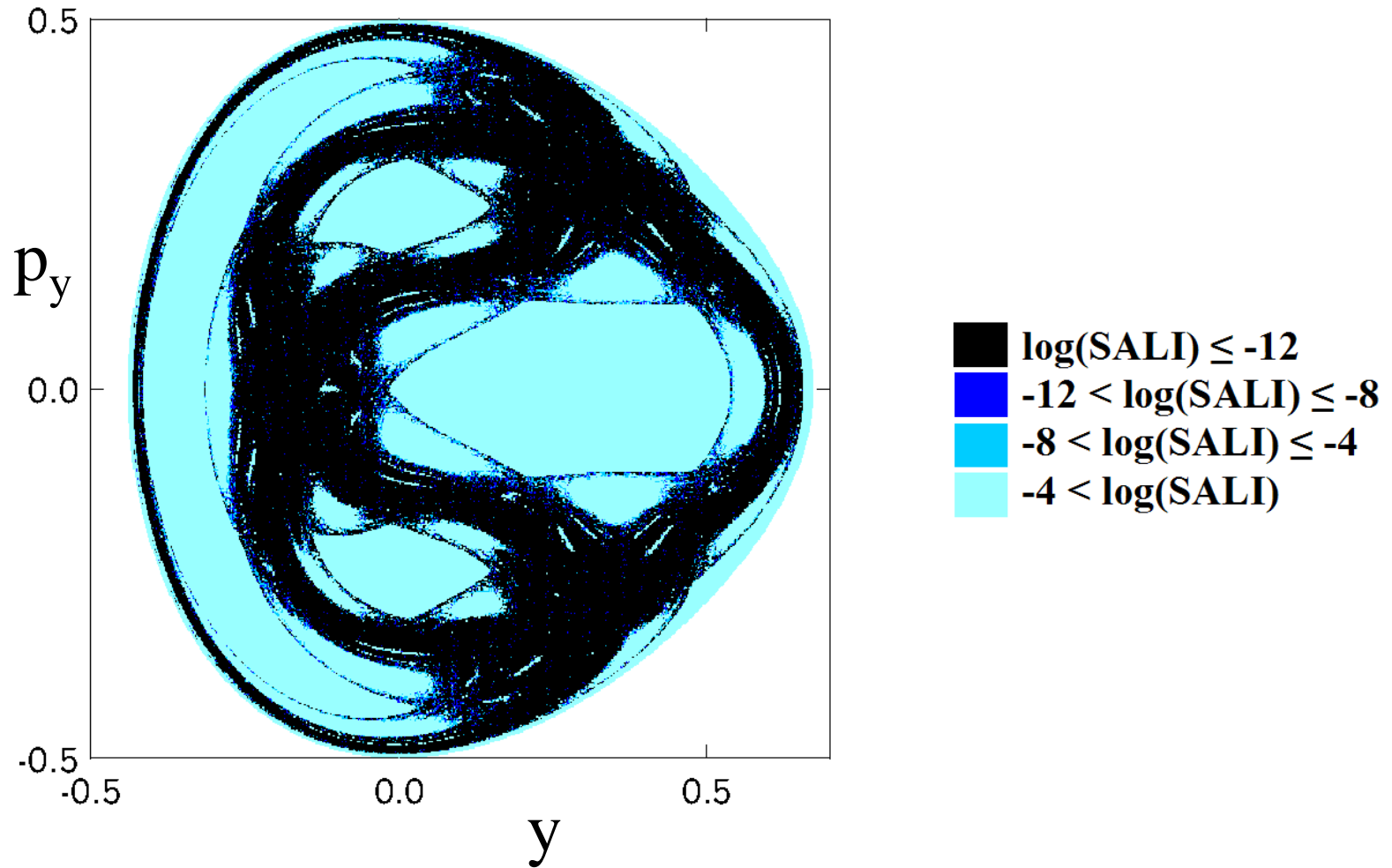
Regular orbit,  $x=0$ ,  $y=0.55$ ,  $p_x=0.2417$ ,  $p_y=0$

Chaotic orbit,  $x=0$ ,  $y=-0.016$ ,  $p_x=0.49974$ ,  $p_y=0$

Chaotic orbit,  $x=0$ ,  $y=-0.01344$ ,  $p_x=0.49982$ ,  $p_y=0$



# SALI – Hénon-Heiles system



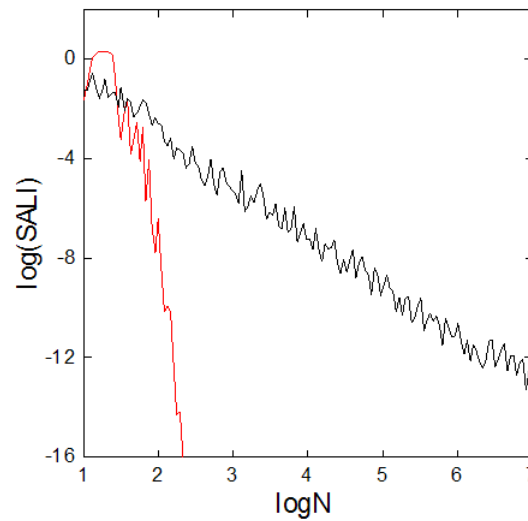
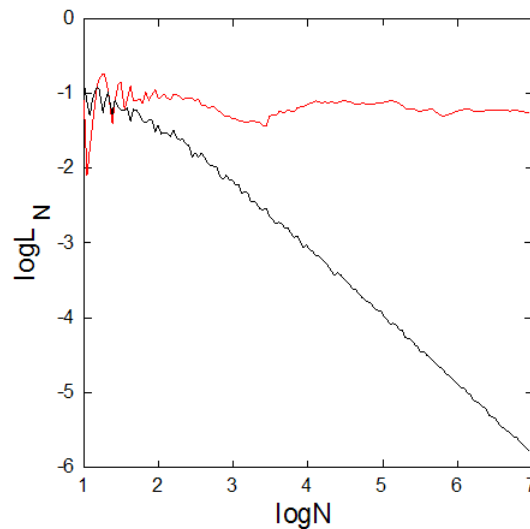
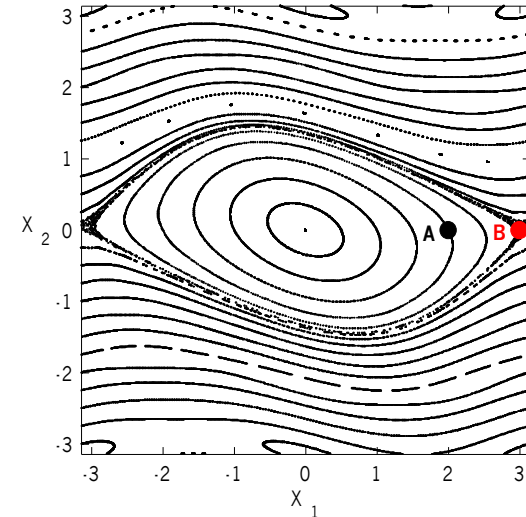
# Applications – 2D map

$$\begin{aligned} \mathbf{x}'_1 &= \mathbf{x}_1 + \mathbf{x}_2 \\ \mathbf{x}'_2 &= \mathbf{x}_2 - \nu \sin(\mathbf{x}_1 + \mathbf{x}_2) \end{aligned} \quad (\text{mod } 2\pi)$$

For  $\nu=0.5$  we consider the orbits:

*regular orbit A* with initial conditions  $x_1=2, x_2=0$ .

*chaotic orbit B* with initial conditions  $x_1=3, x_2=0$ .



# Behavior of the SALI

## 2D maps

SALI  $\rightarrow 0$  both for regular and chaotic orbits

following, however, completely different time rates which allows us to distinguish between the two cases.

## Hamiltonian flows and multidimensional maps

SALI  $\rightarrow 0$  for chaotic orbits

SALI  $\rightarrow \text{constant} \neq 0$  for regular orbits

# **The Generalized ALignment Indices (GALIs) method**

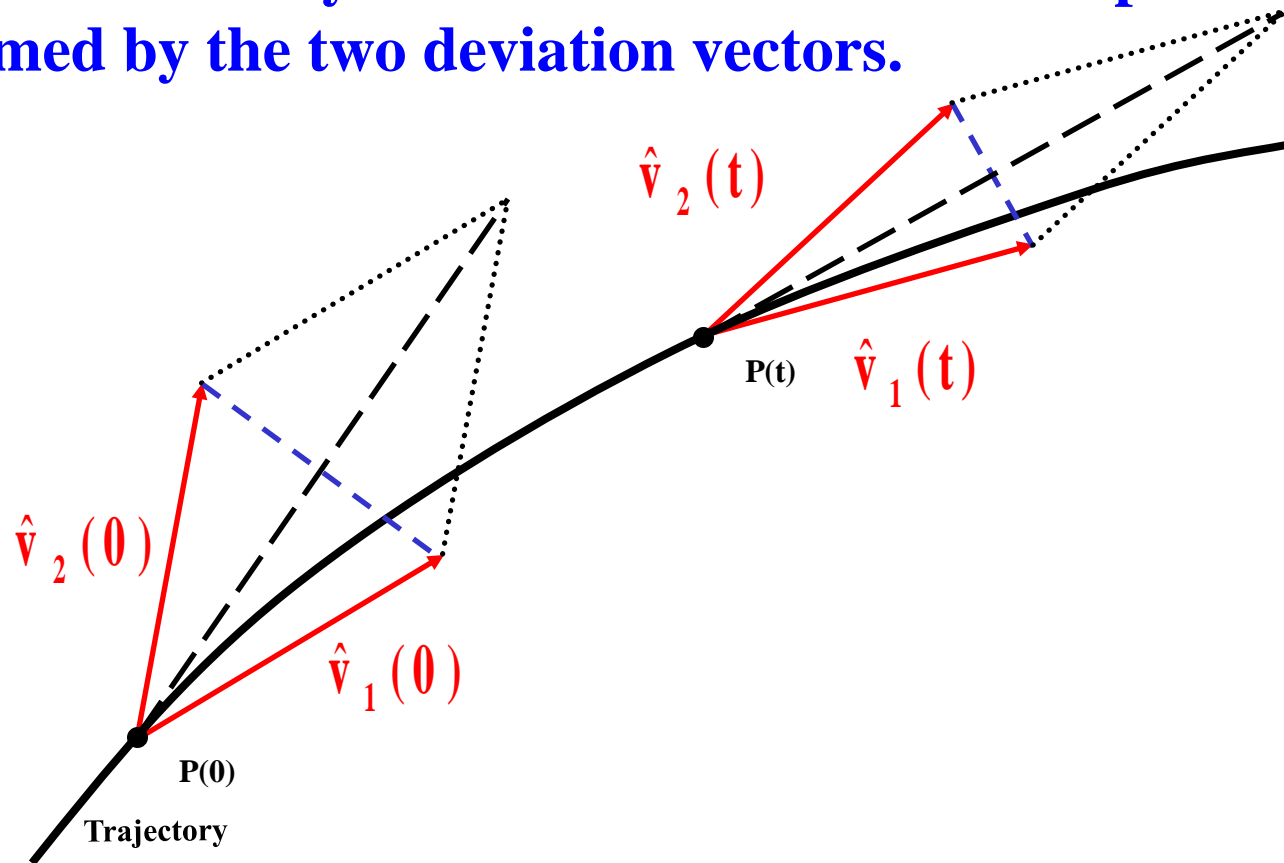


# Definition of the Generalized Alignment Index (GALI)

**SALI effectively measures the 'area' of the parallelogram formed by the two deviation vectors.**

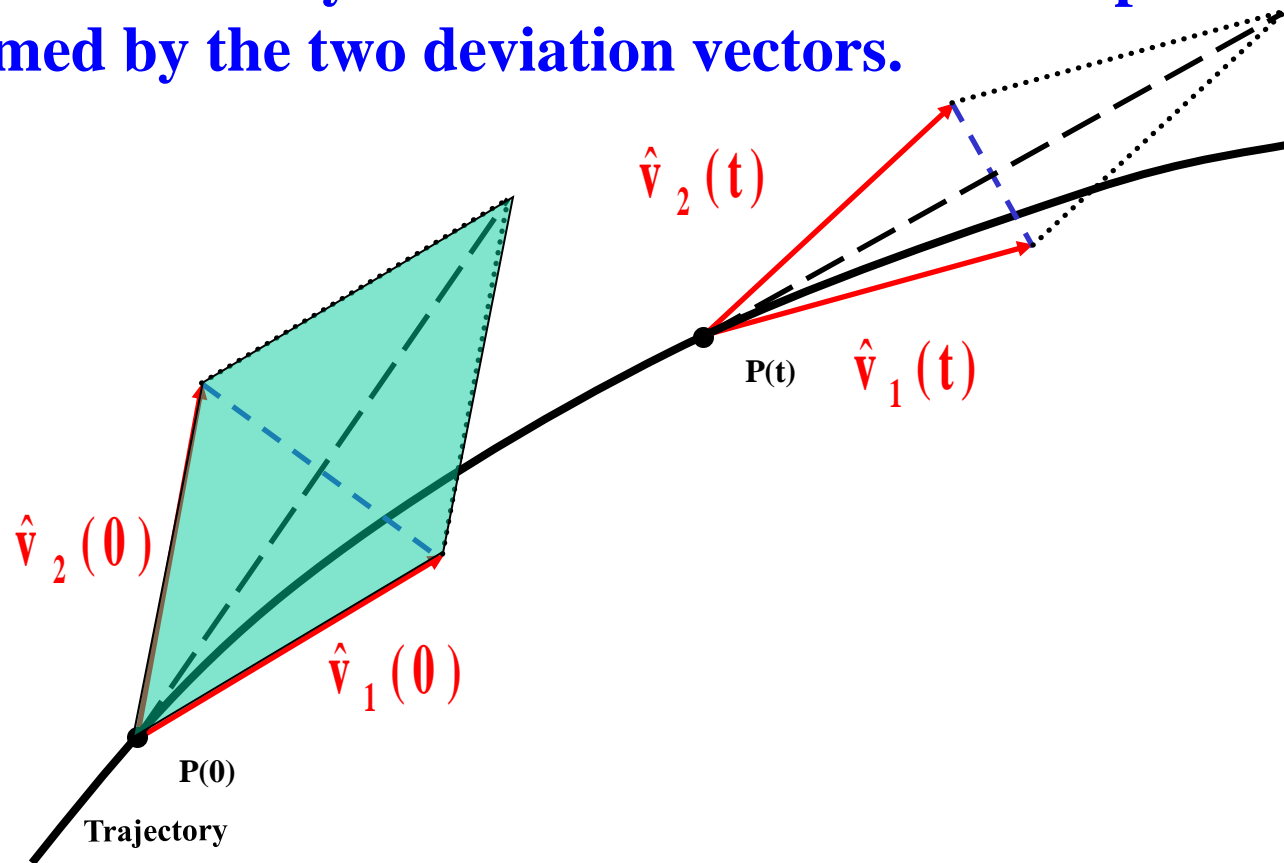
# Definition of the Generalized Alignment Index (GALI)

SALI effectively measures the 'area' of the parallelogram formed by the two deviation vectors.



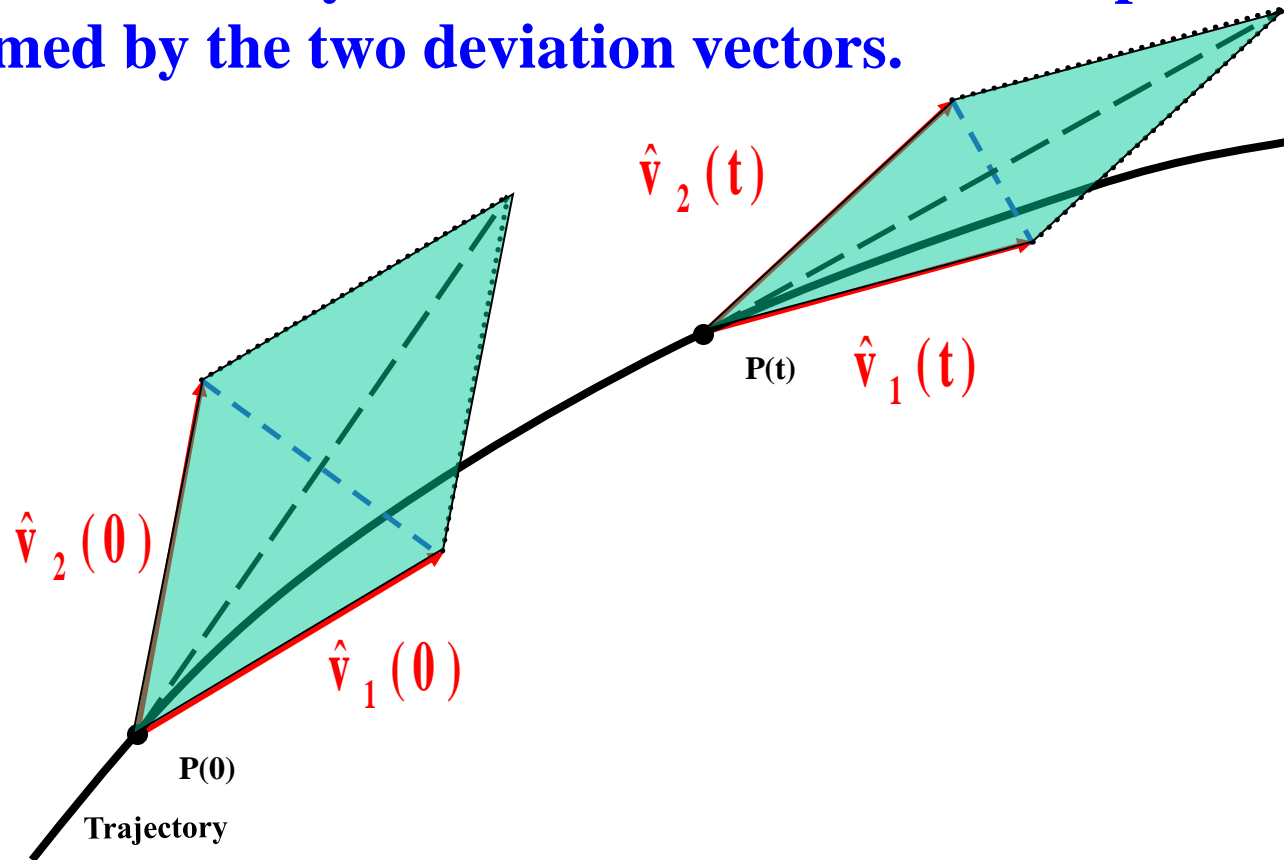
# Definition of the Generalized Alignment Index (GALI)

SALI effectively measures the 'area' of the parallelogram formed by the two deviation vectors.



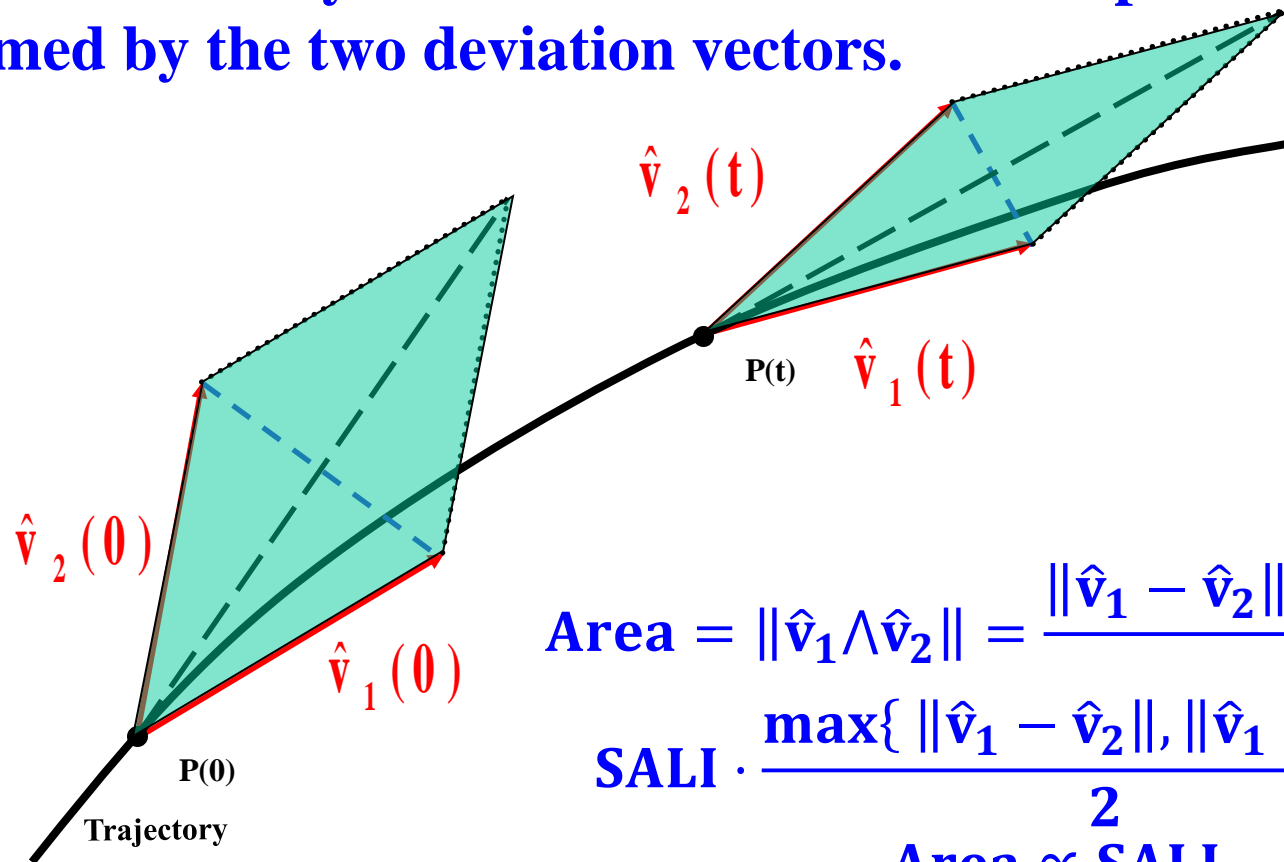
# Definition of the Generalized Alignment Index (GALI)

SALI effectively measures the 'area' of the parallelogram formed by the two deviation vectors.



# Definition of the Generalized Alignment Index (GALI)

SALI effectively measures the ‘area’ of the parallelogram formed by the two deviation vectors.



$$\text{Area} = \|\hat{\mathbf{v}}_1 \wedge \hat{\mathbf{v}}_2\| = \frac{\|\hat{\mathbf{v}}_1 - \hat{\mathbf{v}}_2\| \cdot \|\hat{\mathbf{v}}_1 + \hat{\mathbf{v}}_2\|}{2} =$$

$$\text{SALI} \cdot \frac{\max\{\|\hat{\mathbf{v}}_1 - \hat{\mathbf{v}}_2\|, \|\hat{\mathbf{v}}_1 + \hat{\mathbf{v}}_2\|\}}{2} \Rightarrow$$

$$\text{Area} \propto \text{SALI}$$

# Definition of the Generalized Alignment Index (GALI)

In the case of an  $N$  degree of freedom Hamiltonian system we follow the evolution of  $k$  deviation vectors with  $2 \leq k \leq 2N$ , and define [S. et al., Physica D (2007)] the Generalized Alignment Index (GALI) of order  $k$ :

$$\text{GALI}_k(t) = \|\hat{\mathbf{v}}_1(t) \wedge \hat{\mathbf{v}}_2(t) \wedge \dots \wedge \hat{\mathbf{v}}_k(t)\|$$

where

$$\hat{\mathbf{v}}_1(t) = \frac{\mathbf{v}_1(t)}{\|\mathbf{v}_1(t)\|}.$$

Note that  $\text{GALI}_2$  ( $k=2$ ) is equivalent to the Smaller Alignment Index (SALI).

# Behavior of the $\text{GALI}_k$

**Chaotic motion:**  $\text{GALI}_k$  ( $2 \leq k \leq 2N$ ) tends exponentially to zero with exponents which involve the values of the first  $k$  largest Lyapunov exponents  $\lambda_1, \lambda_2, \dots, \lambda_k$ :

$$\text{GALI}_k(t) \propto e^{-[(\lambda_1 - \lambda_2) + (\lambda_1 - \lambda_3) + \dots + (\lambda_1 - \lambda_k)]t}$$

**Regular motion:** When the motion occurs on an  $N$ -dimensional torus then the behavior of  $\text{GALI}_k$  is given by [S. et al., Physica D (2007) – S. et al., Eur. Phys. J. Sp. Top. (2008)]:

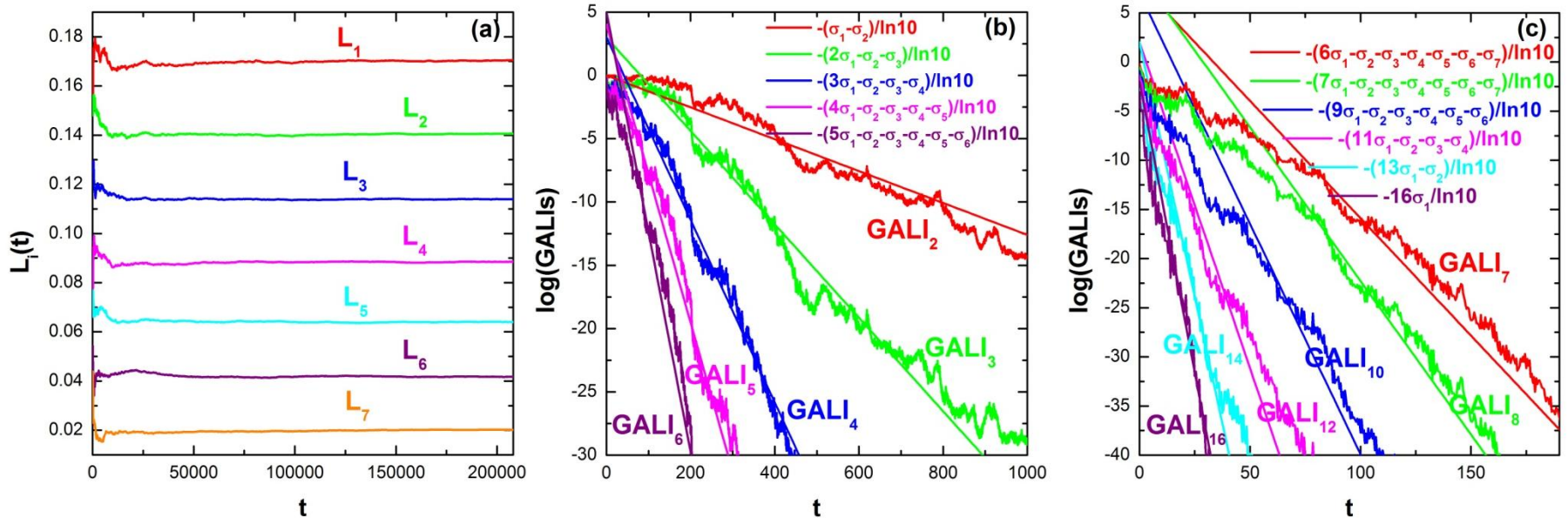
$$\text{GALI}_k(t) \propto \begin{cases} \text{constant} & \text{if } 2 \leq k \leq N \\ \frac{1}{t^{2(k-N)}} & \text{if } N < k \leq 2N \end{cases}$$

# Behavior of the $GALI_k$ for **chaotic motion**

**N particles Fermi-Pasta-Ulam-Tsingou (FPUT) system:**

$$H = \frac{1}{2} \sum_{i=1}^N p_i^2 + \sum_{i=0}^N \left[ \frac{1}{2} (q_{i+1} - q_i)^2 + \frac{\beta}{4} (q_{i+1} - q_i)^4 \right]$$

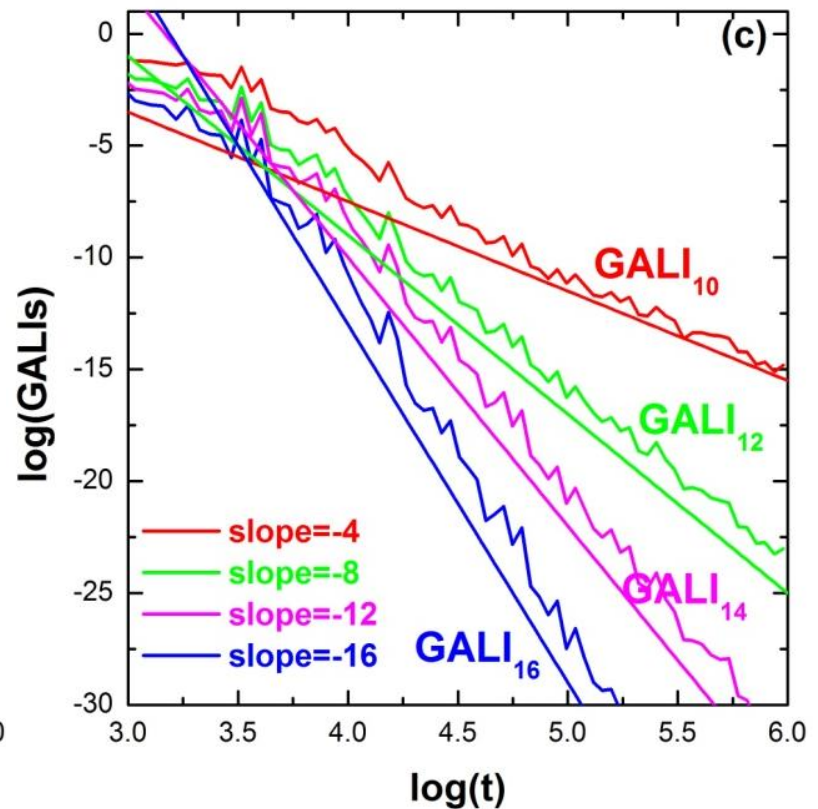
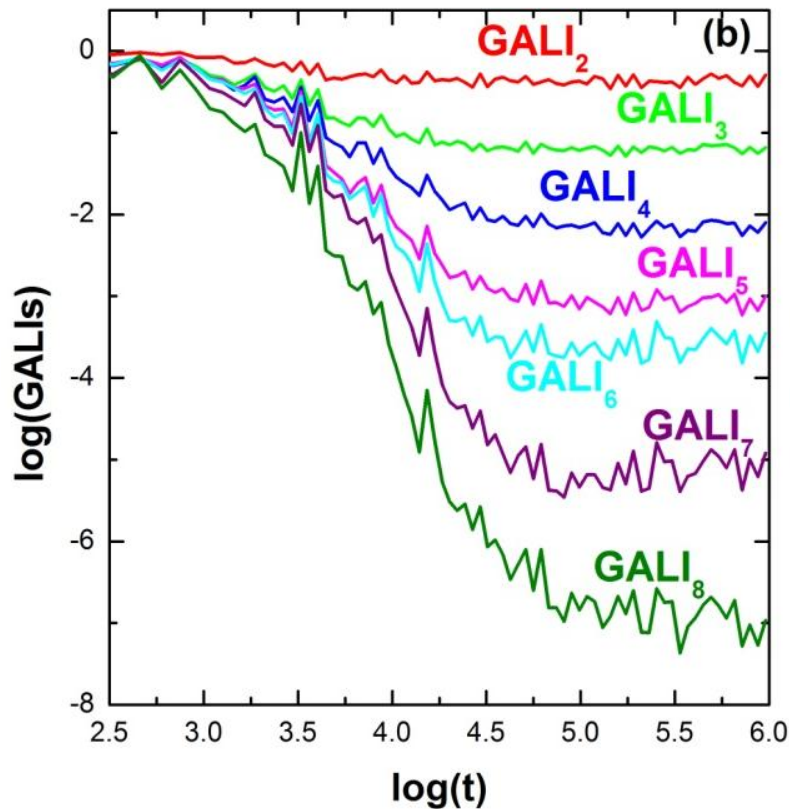
with fixed boundary conditions,  $N=8$  and  $\beta=1.5$ .





# Behavior of the $GALI_k$ for regular motion

N=8 FPUT system



# Global dynamics

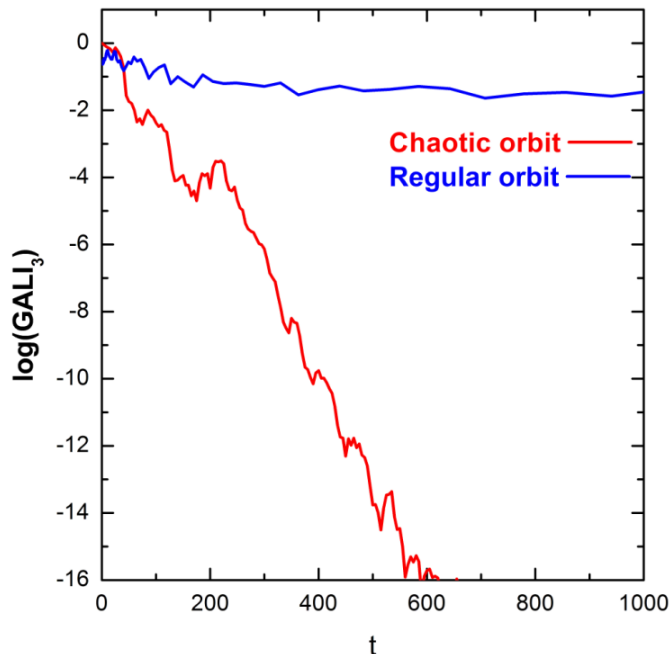
- $\text{GALI}_2$  (practically equivalent to the use of SALI)

- $\text{GALI}_N$

**Chaotic motion:  $\text{GALI}_N \rightarrow 0$   
(exponential decay)**

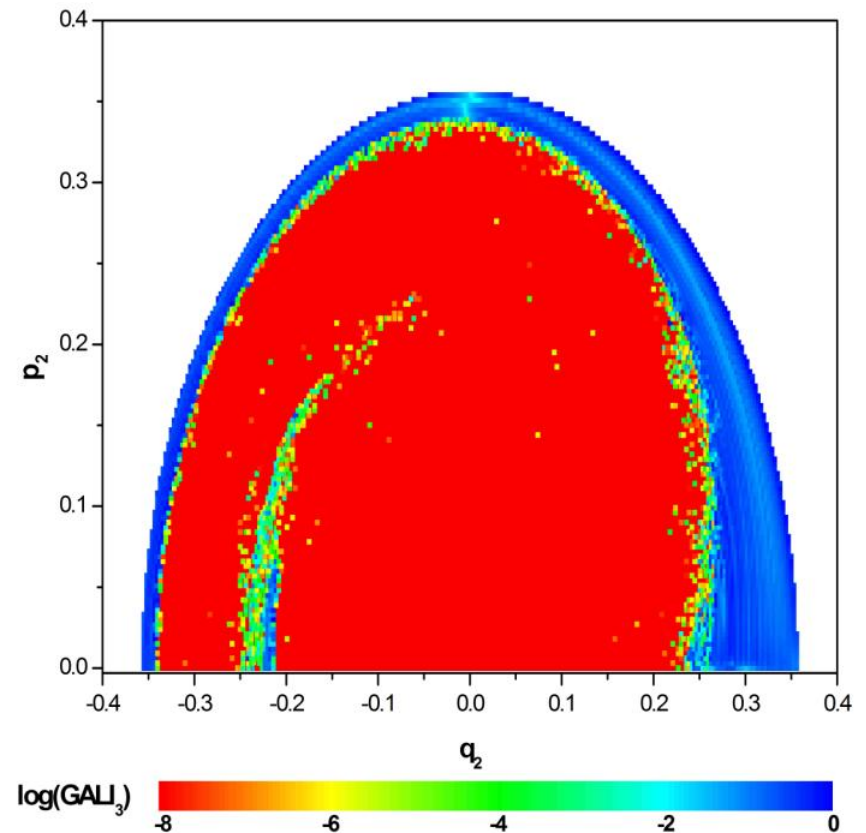
**Regular motion:**

**$\text{GALI}_N \approx \text{constant} \neq 0$**



**3D Hamiltonian**

**Subspace  $q_3=p_3=0$ ,  $p_2 \geq 0$  for  $t=1000$ .**



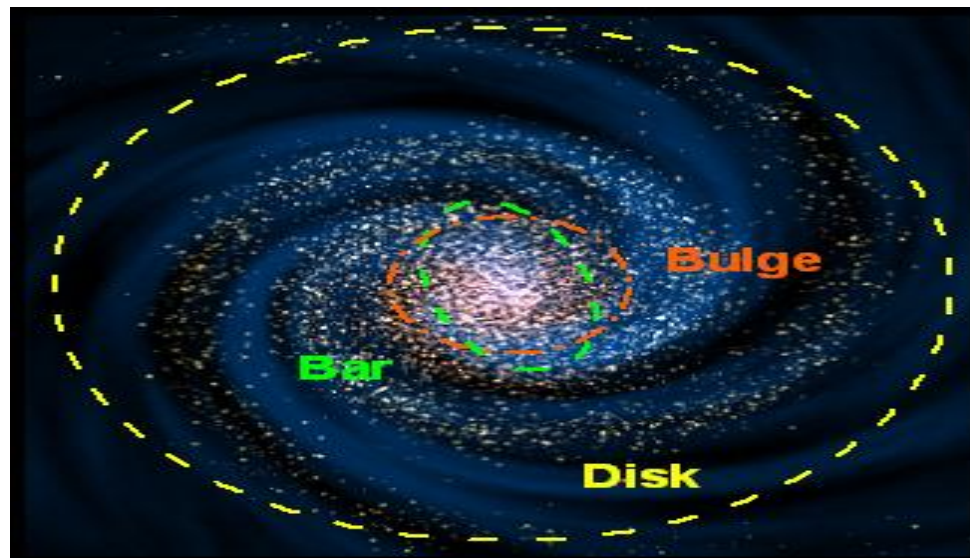
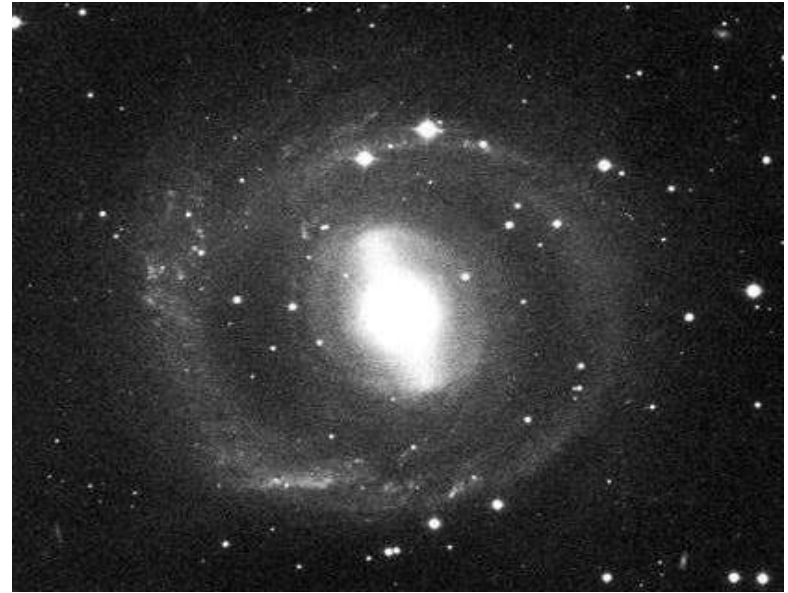
# **A time-dependent Hamiltonian system**

# Barred galaxies

NGC 1433



NGC 2217



# Barred galaxy model

The 3D bar rotates around its short  $z$ -axis ( $x$ : long axis and  $y$ : intermediate). The Hamiltonian that describes the motion for this model is:

$$H = \frac{1}{2}(p_x^2 + p_y^2 + p_z^2) + V(x, y, z) - \Omega_b(xp_y - yp_x) \equiv \text{Energy}$$

This model consists of the superposition of potentials describing an **axisymmetric** part and a **bar** component of the galaxy [Manos et al., J. Phys. A (2013)].

**a) Axisymmetric component:**

i) **Plummer sphere:**

$$V_{\text{sphere}}(x, y, z) = -\frac{GM_s}{\sqrt{x^2 + y^2 + z^2 + \epsilon_s^2}}$$

ii) **Miyamoto–Nagai disc:**

$$V_{\text{disc}}(x, y, z) = -\frac{GM_D}{\sqrt{x^2 + y^2 + (A + \sqrt{B^2 + z^2})^2}}$$

**b) Bar component:**  $V_{\text{bar}}(x, y, z) = -\pi Gabc \frac{\rho_c}{n+1} \int_{\lambda}^{\infty} \frac{du}{\Delta(u)} (1 - m^2(u))^{n+1},$

**(Ferrers bar)**

$$\rho_c = \frac{105}{32\pi} \frac{GM_B}{abc}$$

$$\text{where } m^2(u) = \frac{x^2}{a^2 + u} + \frac{y^2}{b^2 + u} + \frac{z^2}{c^2 + u}, \Delta^2(u) = (a^2 + u)(b^2 + u)(c^2 + u),$$

$n$ : positive integer ( $n = 2$  for our model),  $\lambda$ : the unique positive solution of  $m^2(\lambda) = 1$

**Its density is:**

$$\rho = \begin{cases} \rho_c (1 - m^2)^n, & \text{for } m \leq 1 \\ 0, & \text{for } m > 1 \end{cases}, \text{ where } m^2 = \frac{x^2}{a^2} + \frac{y^2}{b^2} + \frac{z^2}{c^2}, a > b > c \text{ and } n = 2.$$

# Time-dependent barred galaxy model

The 3D bar rotates around its short  $z$ -axis ( $x$ : long axis and  $y$ : intermediate). The Hamiltonian that describes the motion for this model is:

$$H = \frac{1}{2}(p_x^2 + p_y^2 + p_z^2) + V(x, y, z, t) - \Omega_b(xp_y - yp_x) \equiv \text{Energy}$$

This model consists of the superposition of potentials describing an **axisymmetric** part and a **bar** component of the galaxy [Manos et al., J. Phys. A (2013)].

**a) Axisymmetric component:**

$$M_S + M_B(t) + M_D(t) = 1, \text{ with } M_B(t) = M_B(0) + \alpha t$$

i) **Plummer sphere:**

$$V_{\text{sphere}}(x, y, z) = -\frac{GM_S}{\sqrt{x^2 + y^2 + z^2 + \epsilon_s^2}}$$

ii) **Miyamoto–Nagai disc:**

$$V_{\text{disc}}(x, y, z) = -\frac{GM_D(t)}{\sqrt{x^2 + y^2 + (A + \sqrt{B^2 + z^2})^2}}$$

**b) Bar component:**  $V_{\text{bar}}(x, y, z) = -\pi Gabc \frac{\rho_c}{n+1} \int_{\lambda}^{\infty} \frac{du}{\Delta(u)} (1 - m^2(u))^{n+1},$

**(Ferrers bar)**

$$\rho_c = \frac{105}{32\pi} \frac{GM_B(t)}{abc}$$

$$\text{where } m^2(u) = \frac{x^2}{a^2 + u} + \frac{y^2}{b^2 + u} + \frac{z^2}{c^2 + u}, \Delta^2(u) = (a^2 + u)(b^2 + u)(c^2 + u),$$

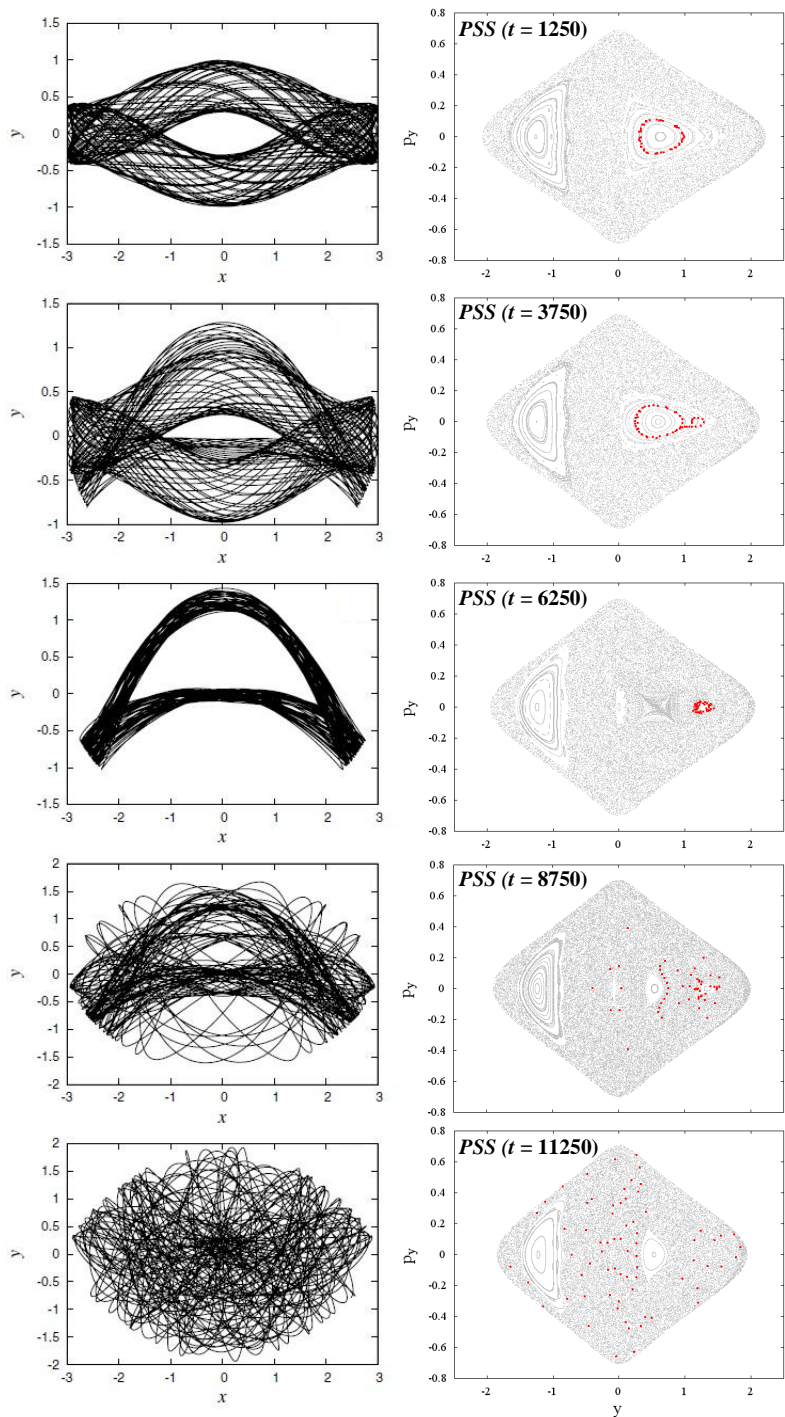
$n$ : positive integer ( $n = 2$  for our model),  $\lambda$ : the unique positive solution of  $m^2(\lambda) = 1$

**Its density is:**

$$\rho = \begin{cases} \rho_c (1 - m^2)^n, & \text{for } m \leq 1 \\ 0, & \text{for } m > 1 \end{cases}, \text{ where } m^2 = \frac{x^2}{a^2} + \frac{y^2}{b^2} + \frac{z^2}{c^2}, a > b > c \text{ and } n = 2.$$



# Time-dependent 2D barred galaxy model



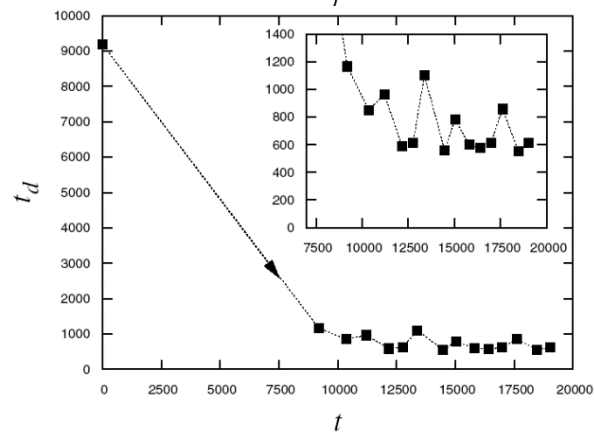
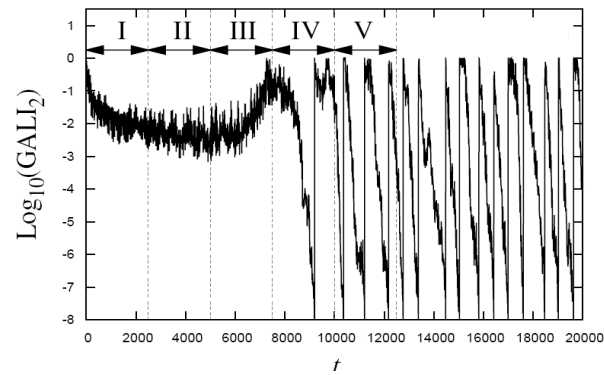
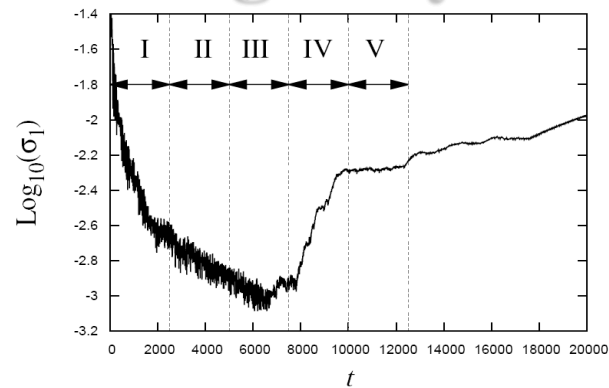
I

II

III

IV

V



# **A dissipative dynamical system**



# Lorenz system

We consider [Moges et al, IJBC in press, nlin.CD/2503.01784 (2025)] orbits leading to different dynamical behaviors for the 3D **Lorenz system** [Lorenz, J. Atmos. Sci. (1963)]:

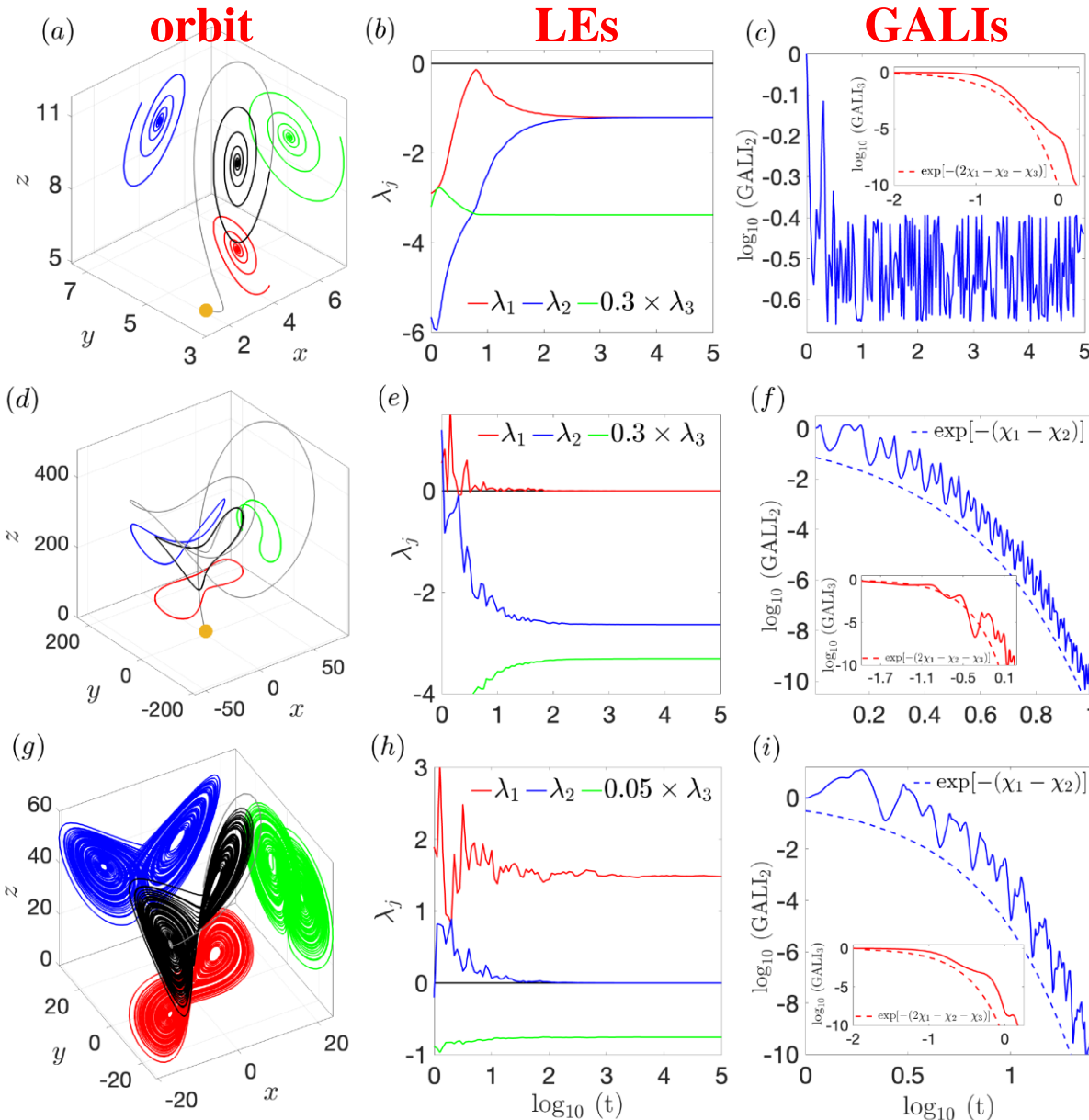
$$\begin{aligned}\frac{dx}{dt} &= a(y - x) \\ \frac{dy}{dt} &= rx - y - xz \\ \frac{dz}{dt} &= xy - bz\end{aligned}$$

In all cases  $\text{GALI}_k$ ,  $k=2, 3$ , follows the evolution defined by:

$$\text{GALI}_k(t) \propto e^{-[(\lambda_1 - \lambda_2) + \dots + (\lambda_1 - \lambda_k)]t}$$

# Lorenz system

We study the orbit with initial condition  $(x, y, z) = (1, 3, 6)$  for  $a = 10$ ,  $b = 8/3$ .



**$r = 2.1$**   
**stable fixed point**

**$r = 1.0$**   
**stable limit cycle**

**$r = 33.3$**   
**chaotic attractor**

# **Chaos diagnostics based on Lagrangian descriptors (LDs)**

# Lagrangian descriptors (LDs)

The computation of LDs is based on the accumulation of some positive scalar value along the path of individual orbits.

Consider an  $N$  dimensional continuous time dynamical system

$$\dot{\mathbf{x}} = \frac{d\mathbf{x}(t)}{dt} = \mathbf{f}(\mathbf{x}, t)$$

**The Arclength Definition** [Madrid & Mancho, Chaos (2009) – Mendoza & Mancho, PRL (2010) – Mancho et al., Commun. Nonlin. Sci. Num. Simul. (2013)].

**Forward time LD:**

$$\text{LD}^f(\mathbf{x}, \tau) = \int_0^\tau \|\dot{\mathbf{x}}(t)\| dt$$

**Backward time LD:**

$$\text{LD}^b(\mathbf{x}, \tau) = \int_{-\tau}^0 \|\dot{\mathbf{x}}(t)\| dt$$

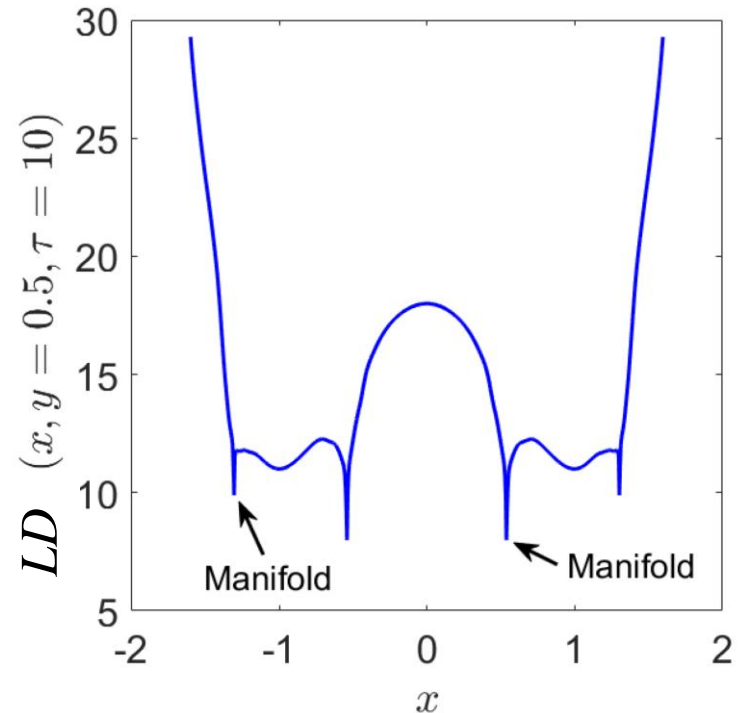
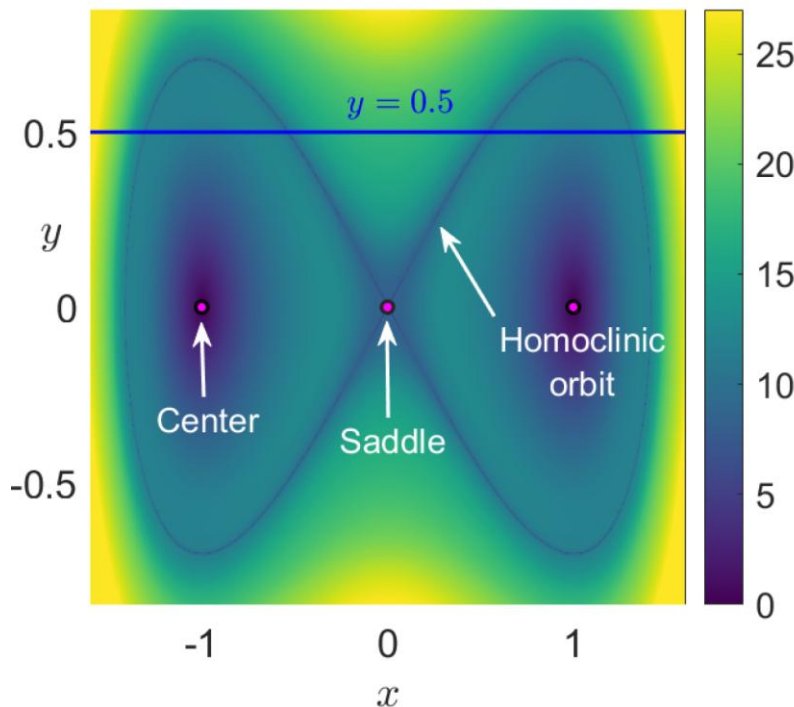
**Combined LD:**

$$\text{LD}(\mathbf{x}, \tau) = \text{LD}^b(\mathbf{x}, \tau) + \text{LD}^f(\mathbf{x}, \tau)$$

# LDs: 1 dof Duffing Oscillator

$$H(x, y) = \frac{1}{2}y^2 + \frac{1}{4}x^4 - \frac{1}{2}x^2$$

The system has three equilibrium points: a saddle located at the origin and two diametrically opposed centers at the points  $(\pm 1, 0)$ .



From Agaoglou et al. 'Lagrangian descriptors: Discovery and quantification of phase space structure and transport', 2020, <https://doi.org/10.5281/zenodo.3958985>

The **location of the stable and unstable manifolds** can be extracted from the ridges of the **gradient field of the LDs** since they are located at points where the forward and the backward components of the LD are non-differentiable.

# Lagrangian descriptors (LDs)

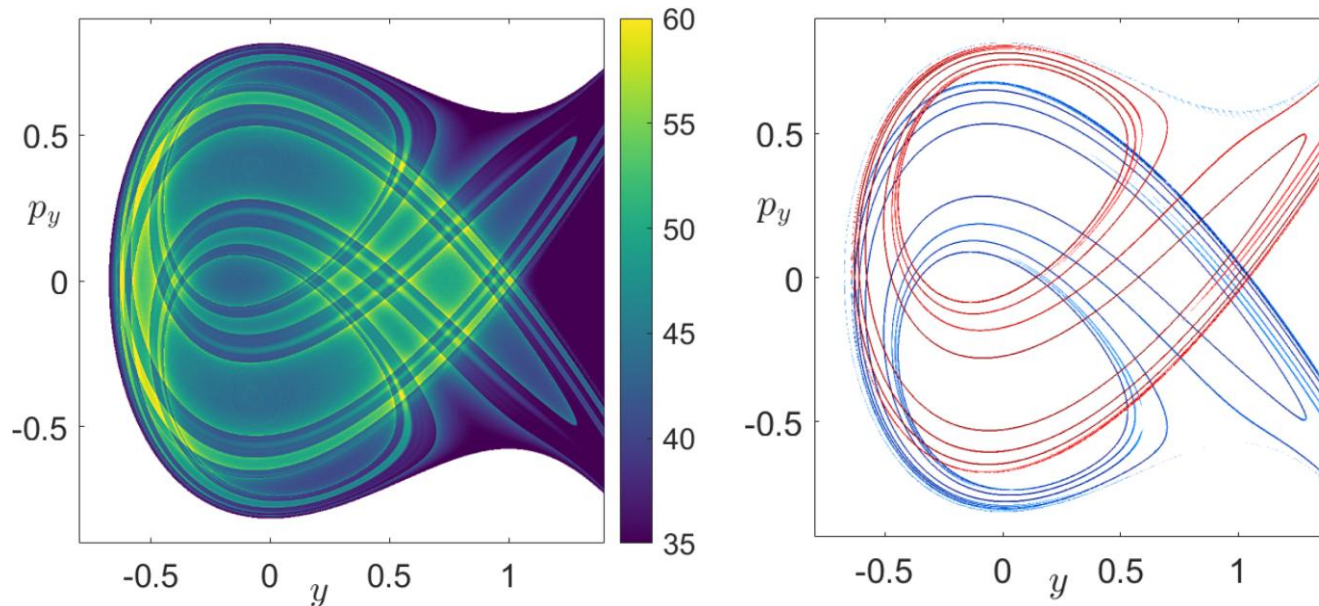
**The ‘p-norm’ Definition** [Lopesino et al., Commun. Nonlin. Sci. Num. Simul. (2015) – Lopesino et al., Int. J. Bifurc. Chaos (2017)].

**Combined LD** (usually  $p=1/2$ ):

$$\text{LD}(\mathbf{x}, \tau) = \int_{-\tau}^{\tau} \left( \sum_{i=1}^N |\mathbf{f}_i(\mathbf{x}, t)|^p \right) dt$$

**Hénon-Heiles system:**  $H = \frac{1}{2}(\mathbf{p}_x^2 + \mathbf{p}_y^2) + \frac{1}{2}(\mathbf{x}^2 + \mathbf{y}^2) + \mathbf{x}^2\mathbf{y} - \frac{1}{3}\mathbf{y}^3$

**Stable** and **unstable** manifolds for  $H=1/3$ ,  $\tau=10$ .



# Using LDs to quantify chaos

We consider orbits on a finite **grid of an  $n(\geq 1)$ -dimensional subspace** of the  **$N(\geq n)$ -dimensional phase space** of a dynamical system and their LDs.

Any non-boundary point  $\mathbf{x}$  in this subspace has  **$2n$  nearest neighbors**

$$\mathbf{y}_i^{\pm} = \mathbf{x} \pm \sigma^{(i)} \mathbf{e}^{(i)}, \quad i = 1, 2, \dots, n,$$

where  $\mathbf{e}^{(i)}$  is the  $i$ th usual basis vector in  $\mathbb{R}^n$  and  $\sigma^{(i)}$  is the distance between successive grid points in this direction.

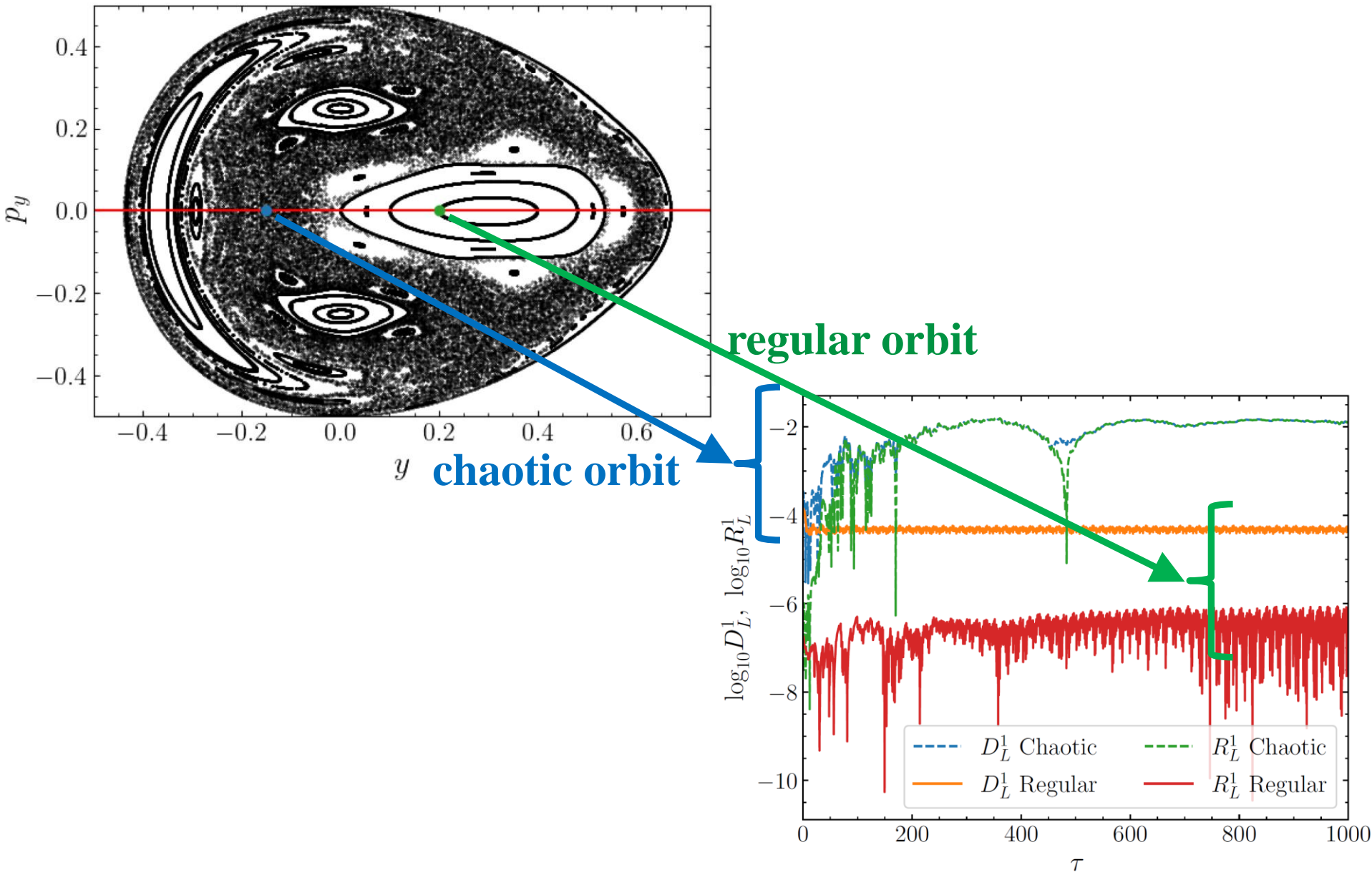
The **difference  $D_L^n$**  of neighboring orbits' LDs:

$$D_L^n(\mathbf{x}) = \frac{1}{2n} \sum_{i=1}^n \frac{|\text{LD}^f(\mathbf{x}) - \text{LD}^f(\mathbf{y}_i^+)| + |\text{LD}^f(\mathbf{x}) - \text{LD}^f(\mathbf{y}_i^-)|}{\text{LD}^f(\mathbf{x})}.$$

The **ratio  $R_L^n$**  of neighboring orbits' LDs:

$$R_L^n(\mathbf{x}) = \left| 1 - \frac{1}{2n} \sum_{i=1}^n \frac{\text{LD}^f(\mathbf{y}_i^+) + \text{LD}^f(\mathbf{y}_i^-)}{\text{LD}^f(\mathbf{x})} \right|.$$

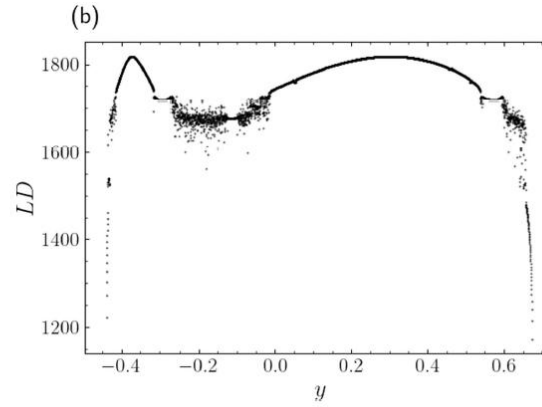
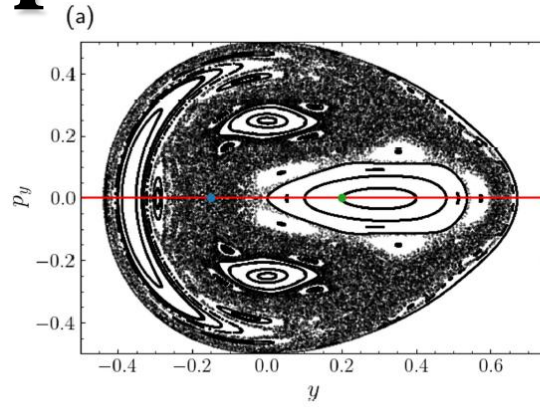
# Application: Hénon-Heiles system





# Application: Hénon-Heiles system

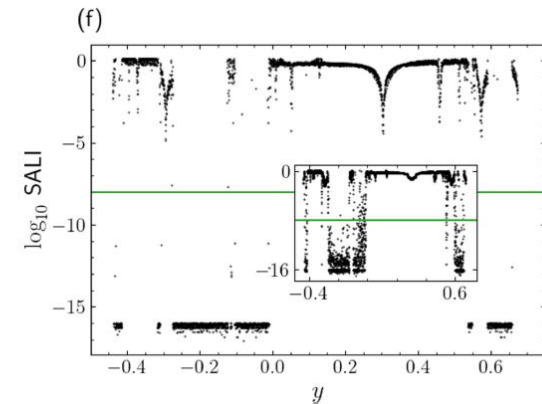
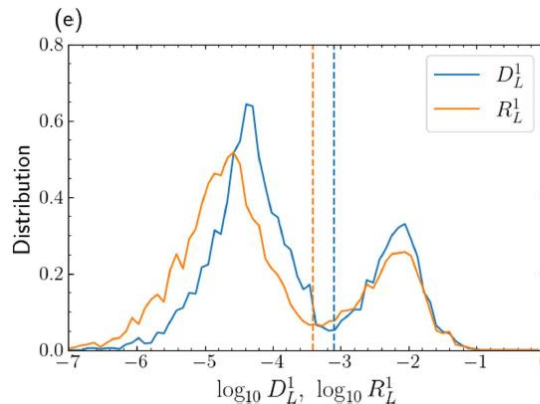
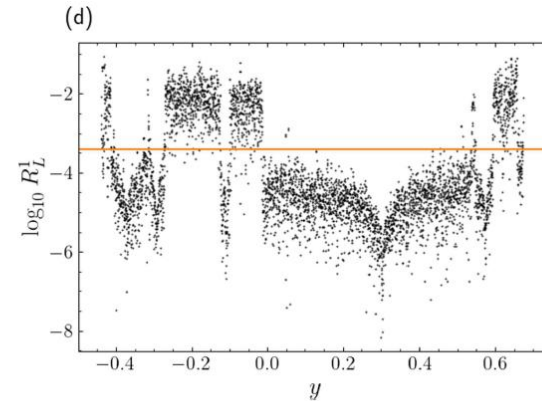
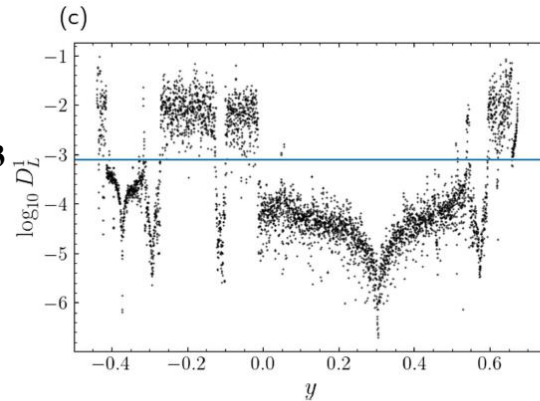
$H=1/8$



Variation of LDs with regard to initial conditions.

**regular regions: smooth**  
**chaotic regions: erratic**

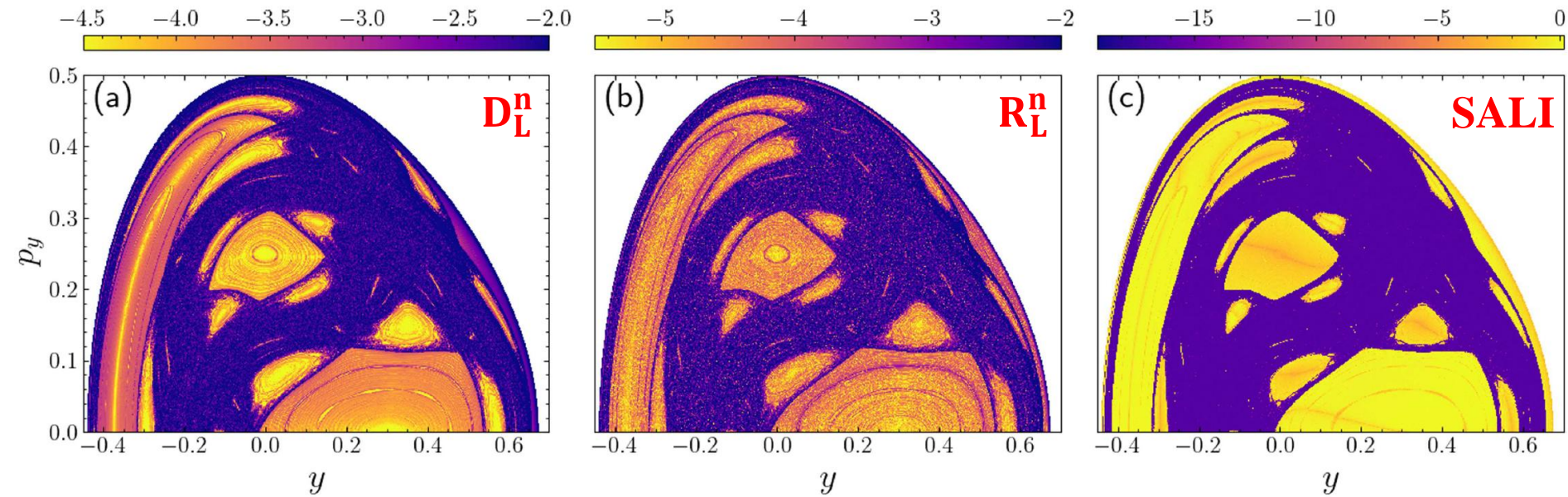
[also see Montes et al., Commun. Nonlin. Sci. Num. Simul. (2021)]



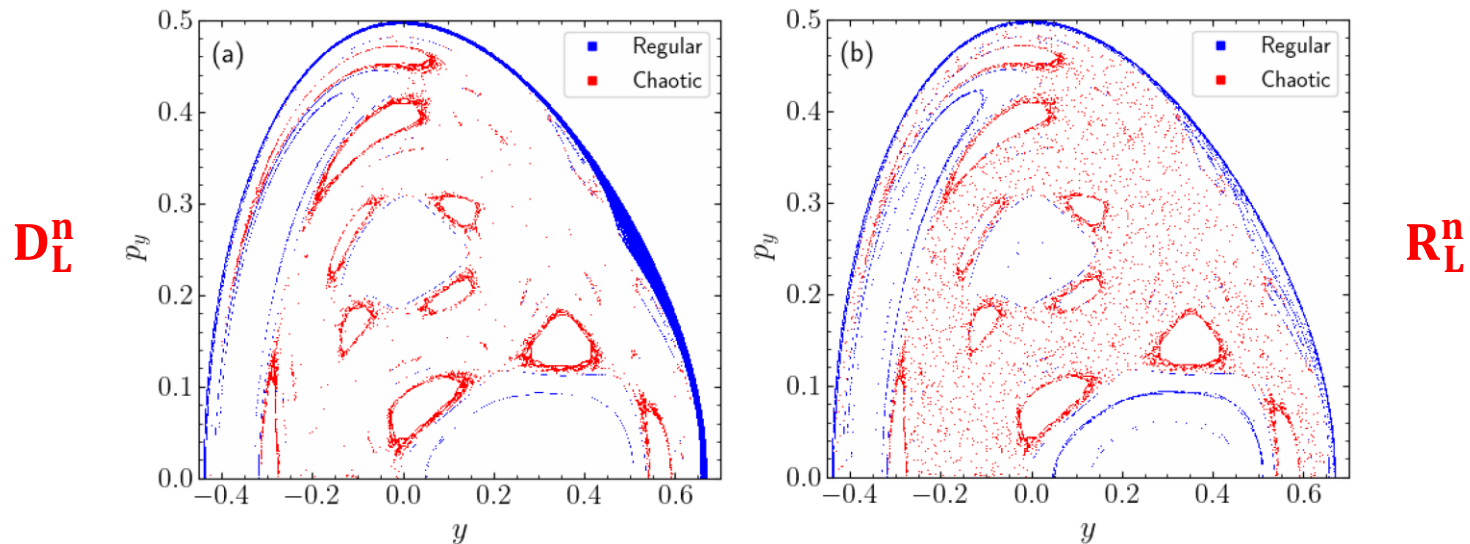
**SALI for  $\tau=10^6$**   
**(inset  $\tau=10^3$ )**

LDs for  $\tau=10^3$

# Application: Hénon-Heiles system



Misclassified orbits (< 10%)





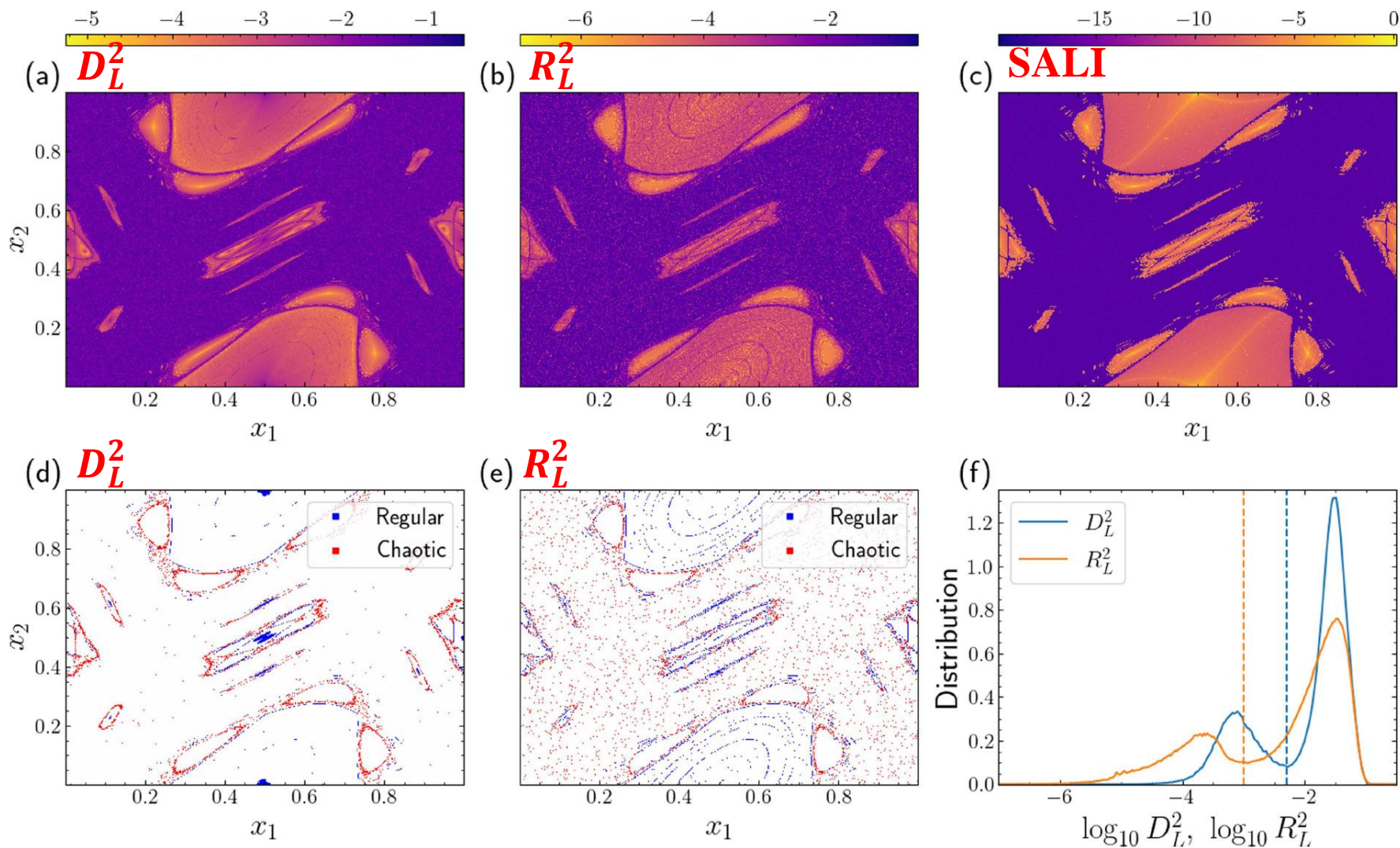
# Application: 2D Standard map

$$\begin{aligned}x'_1 &= x_1 + x'_2 \\x'_2 &= x_2 + \frac{K}{2\pi} \sin(2\pi x_1) \pmod{1}\end{aligned}$$

We set  $K = 1.5$

Thresholds:  $\log_{10} D_L^2 = -2.3$ ,  $\log_{10} R_L^2 = -3$  ( $T = 10^3$ )

$\log_{10} \text{SALI} = -12$  ( $T = 10^5$ )

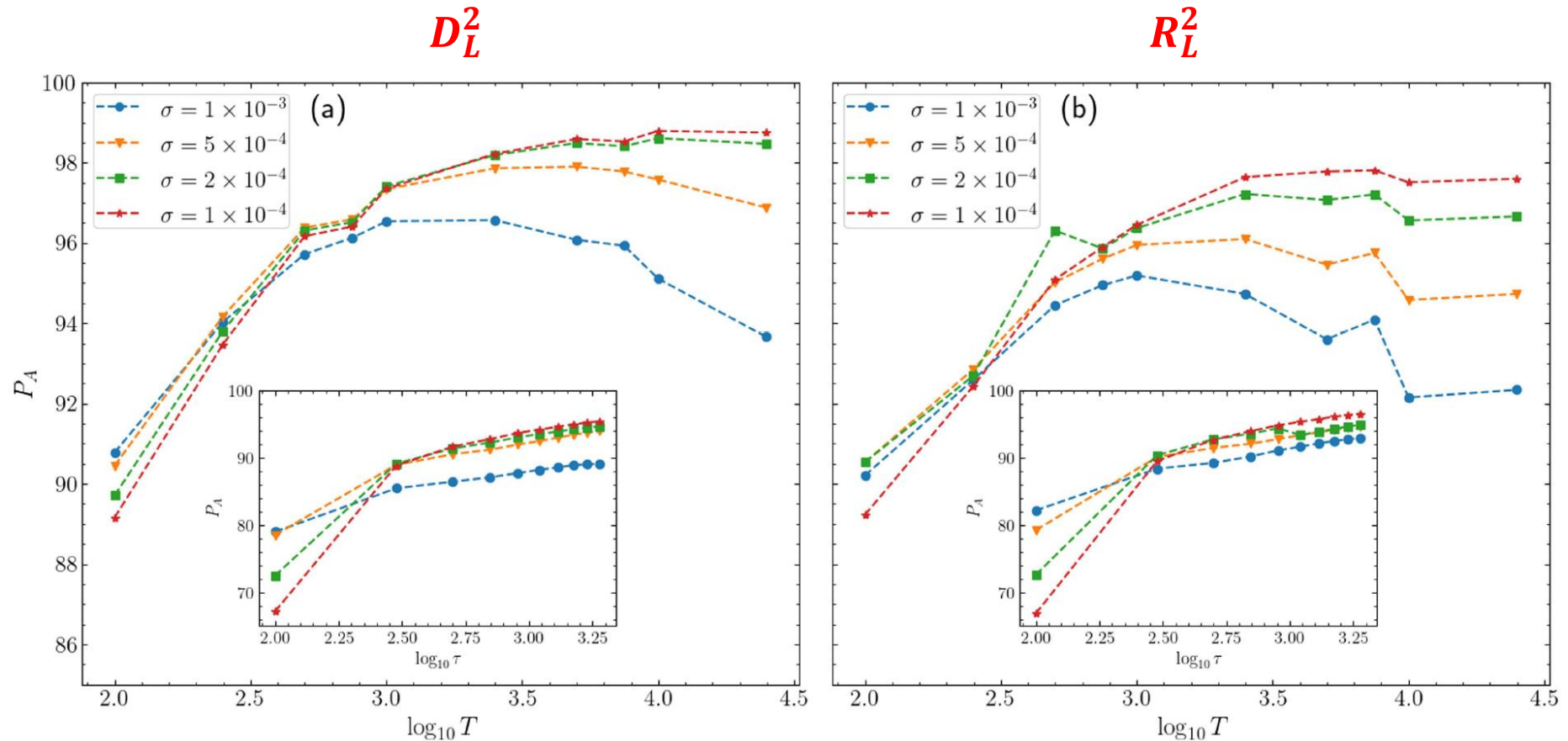


# Effect of grid spacing ( $\sigma$ ) and final integration time ( $T, \tau$ )

$P_A$  : percentage of correctly characterized orbits

Main plots: 2D Standard map

Insets: Hénon-Heiles system



# Summary

- The Smaller (SALI) and the Generalized (GALI) ALignment Index methods are **fast, efficient and easy to compute chaos indicator**.
- Behaviour of the Generalized ALignment Index of order  $k$  ( $GALI_k$ ):
  - ✓ **Chaotic motion: it tends exponentially to zero**
  - ✓ **Regular motion: it fluctuates around non-zero values (or goes to zero following power-laws)**
- $GALI_k$  indices :
  - ✓ **can distinguish rapidly and with certainty between regular and chaotic motion**
  - ✓ **can be used to characterize individual orbits as well as "chart" chaotic and regular domains in phase space**
  - ✓ **can identify regular motion on low-dimensional tori**
  - ✓ **are perfectly suited for studying the global dynamics of multidimensional systems, as well as of time-dependent models**
  - ✓ **they must be used with care in the case of dissipative systems**
- We introduced and successfully implemented computationally efficient ways to **effectively identify chaos** in conservative dynamical systems **from the values of LDs at neighboring initial conditions**.
  - ✓ **Advantages:**
    - The indices show **overall very good performance**, as their classifications are in accordance with the ones obtained by the SALI at a level of at least 90% agreement.
    - **Easy to compute** (actually only the forward LDs are needed).
    - **No need to know and to integrate the variational equations.**

# Basic References

## **SALI**

S. (2001) J. Phys. A, 34, 10029

S., Antonopoulos, Bountis & Vrahatis (2003) Prog. Theor. Phys. Supp., 150, 439

S., Antonopoulos, Bountis & Vrahatis (2004) J. Phys. A, 37, 6269

## **GALI**

S., Bountis & Antonopoulos (2007) Physica D, 231, 30

S., Bountis & Antonopoulos (2008) Eur. Phys. J. Sp. Top., 165, 5

Manos, S. & Antonopoulos (2012) Int. J. Bifur. Chaos, 22, 1250218

Manos, Bountis & S. (2013) J. Phys. A, 46, 254017

Moges, Manos, Racoveany, S. (2025) Int. J. Bifur. Chaos (in press), arXiv: nlin.CD/2503.01784.

## **Reviews on SALI and GALI**

Bountis & S. (2012) ‘Complex Hamiltonian Dynamics’, Chapter 5, Springer Series in Synergetics

S. & Manos (2016) Lect. Notes Phys., 915, 129

## **Lagrangian descriptors (LDs)**

Madrid & Mancho (2009) Chaos, 19, 013111

Mendoza & Mancho (2010) Phys. Rev. Lett., 105, 038501

Mancho, Wiggins, Curbelo & Mendoza (2013) Com. Nonlin. Sci. Num. Simul., 18, 3530

Montes, Revuelta & Borondo (2021) Com. Nonlin. Sci. Num. Simul., 102, 105860

Daquin, Pédenon-Orlanducci, Agaoglou, García-Sánchez & Mancho (2022) Physica D, 442, 133520

## **Chaos diagnostics based on LDs**

Hillebrand, Zimper, Ngapasare, Katsanikas, Wiggins & S. (2022) Chaos, 32, 123122

Zimper, Ngapasare, Hillebrand, Katsanikas, Wiggins & S. (2023) Physica D, 453, 133833



# A ...shameless promotion

## Contents

Lecture Notes in Physics 915

Charalampos (Haris) Skokos  
Georg A. Gottwald  
Jacques Laskar *Editors*

# Chaos Detection and Predictability

 Springer

1. Parlitz: Estimating Lyapunov Exponents from Time Series
2. Lega, Guzzo, Froeschlé: Theory and Applications of the Fast Lyapunov Indicator (FLI) Method
3. Barrio: Theory and Applications of the Orthogonal Fast Lyapunov Indicator (OFLI and OFLI2) Methods
4. Cincotta, Giordano: Theory and Applications of the Mean Exponential Growth Factor of Nearby Orbits (MEGNO) Method
5. S., Manos: The Smaller (SALI) and the Generalized (GALI) Alignment Indices: Efficient Methods of Chaos Detection
6. Sándor, Maffione: The Relative Lyapunov Indicators: Theory and Application to Dynamical Astronomy
7. Gottwald, Melbourne: The 0-1 Test for Chaos: A Review
8. Siegert, Kantz: Prediction of Complex Dynamics: Who Cares About Chaos?